Constraining long-term denudation and faulting history in intraplate regions by multisystem thermochronology: An example of the Sudetic Marginal Fault (Bohemian Massif, central Europe)

Martin Danišík,[1,2] Petra Štěpančíková,[3] and Noreen J. Evans[2,4]

Received 28 August 2011; revised 24 December 2011; accepted 4 January 2012; published 13 March 2012.

[1] The Rychlebské hory Mountain region in the Sudetes (NE Bohemian Massif) provides a natural laboratory for studies of postorogenic landscape evolution. This work reveals both the exhumation history of the region and the paleoactivity along the Sudetic Marginal Fault (SMF) using zircon (U-Th)/He (ZHe), apatite fission track (AFT), and apatite (U-Th)/He (AHe) dating of crystalline basement and postorogenic sedimentary samples. Most significantly, and in direct contradiction of traditional paleogeographic reconstructions, this work has found evidence of a large Cretaceous sea and regional burial (to >6.5 km) of the Carboniferous-Permian basement in the Late Cretaceous (~95–80 Ma). During the burial by sediments of the Bohemian Cretaceous Basin System, the SMF acted as a normal fault as documented by offset ZHe ages across the fault. At 85–70 Ma, the basin was inverted, Cretaceous strata eroded, and basement blocks were exhumed to the near surface at a rate of ~300 m/Ma as evidenced by Late Cretaceous–Paleocene AFT ages and thermal modeling results. There is no appreciable difference in AFT and AHe ages across the fault, suggesting that the SMF acted as a reverse fault during exhumation. In the late Eocene–Oligocene, the basement was locally heated to <70°C by magmatic activity related to opening of the Eger rift system. Neogene or younger thermal activity was not recorded in the thermochronological data, confirming that late Cenozoic uplift and erosion of the basement blocks was limited to less than ~1.5 km in the study area.

Citation: Danišík, M., P. Štěpančíková, and N. J. Evans (2012), Constraining long-term denudation and faulting history in intraplate regions by multisystem thermochronology: An example of the Sudetic Marginal Fault (Bohemian Massif, central Europe), *Tectonics*, *31*, TC2003, doi:10.1029/2011TC003012.

1. Introduction

[2] In order to elucidate aspects of structural, tectonic and surface processes in older terrains, it is critical that fault history and the timing, rate and extent of exhumation are well understood. This presents challenges, particularly where comprehensive posttectonic sedimentary records or bracketing igneous rocks are lacking and/or where fault systems controlling modern topography are poorly exposed [e.g., *Hejl et al.*, 1997; *Cederbom et al.*, 2000; *Belton et al.*, 2004; *Hendriks and Redfield*, 2005; *Green and Duddy*, 2006; *Danišík et al.*, 2008].

[3] The Bohemian Massif represents the easternmost exposure in a wide belt of late Paleozoic crystalline bodies in Europe called the European Variscides [cf. *McCann*, 2008] and its post-Paleozoic evolution is not clearly understood. Like other crystalline bodies in the European Variscides, the Bohemian Massif was assembled during the Late Devonian–Permian (so-called Variscan) orogeny. The Variscan orogenic evolution of the Bohemian Massif is well constrained by high-temperature geochronometers and thermochronometers (i.e., U/Pb, Pb/Pb, Sm/Nd, Rb/Sr, Ar/Ar, sphene and zircon fission track) [e.g., *Jarmołowicz-Szulc*, 1984; *Kreuzer et al.*, 1989; *Košler et al.*, 1995, 2001; *Kotková et al.*, 1996; *Kröner and Willner*, 1998; *Kröner and Hegner*, 1998; *Propach et al.*, 2000; *Thomson and Zeh*, 2000; *Janoušek et al.*, 2010; *Schulmann et al.*, 2005; *Schneider et al.*, 2006; *Siebel et al.*, 2008; *Awdankiewicz et al.*, 2010]; however, its low-temperature (i.e., <240°C), postorogenic evolution is a matter of debate, particularly due to the sparsely preserved post-Permian geologic record [e.g., *Wagner et al.*, 1997; *Glasmacher et al.*, 2002; *Ventura and Lisker*, 2003; *Filip and Suchý*, 2004; *Aramowicz et al.*, 2006; *Ventura et al.*, 2009; *Danišík et al.*, 2010; *Siebel et al.*, 2010].

[1]Department of Earth and Ocean Sciences, University of Waikato, Hamilton, New Zealand.
[2]John de Laeter Centre for Isotope Research, Applied Geology, Curtin University of Technology, Perth, Western Australia, Australia.
[3]Department of Engineering Geology, Institute of Rock Structure and Mechanics, Academy of Sciences of the Czech Republic, Prague, Czech Republic.
[4]CSIRO Earth Science and Resource Engineering, Kensington, Western Australia, Australia.

0278-7407/12/2011TC003012

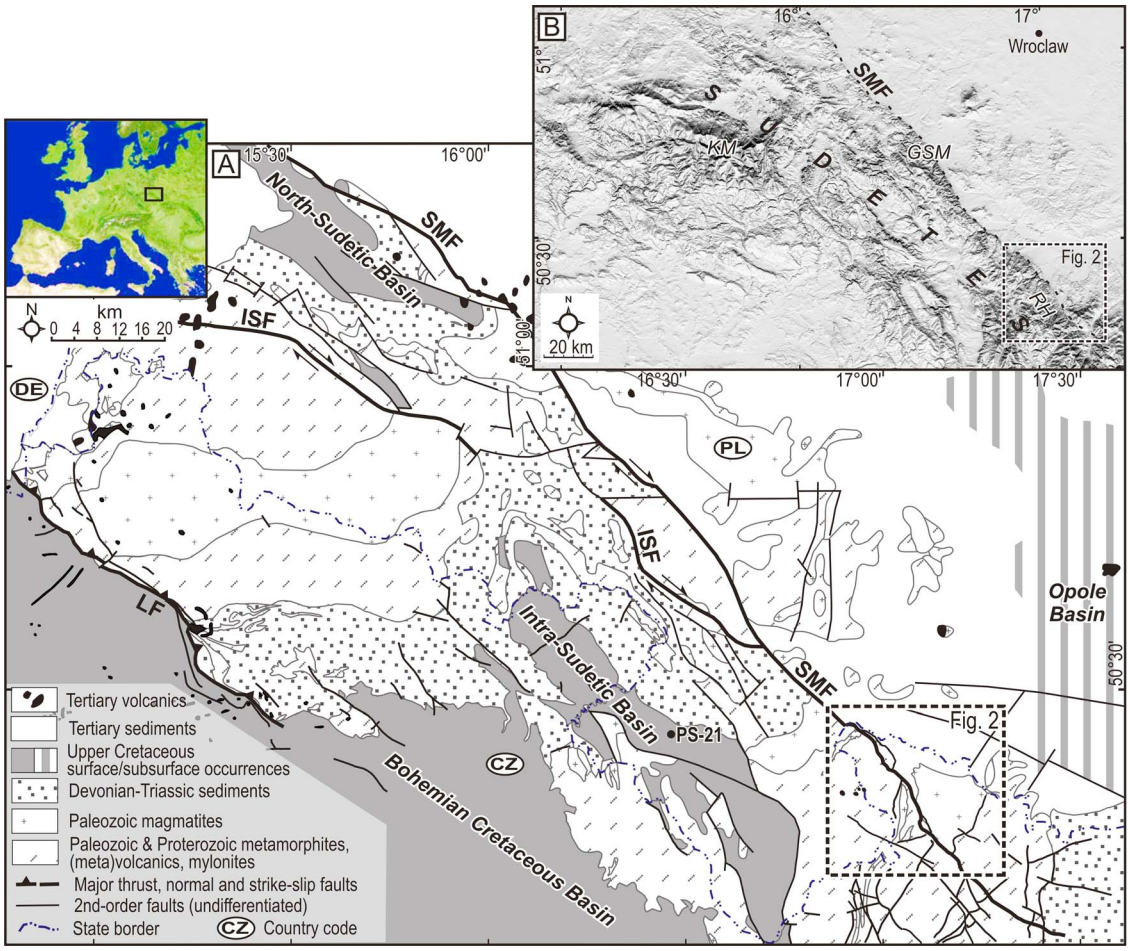

Figure 1. (inset) Position of the Sudetes in Europe (black rectangle). (a) Simplified geological map of the Sudetes (modified after *Cymerman* [2004] and *Czech Geological Survey* [1998]) with position of the main study area and location of Cretaceous sandstone sample (PS-21) collected in the Intra-Sudetic Basin. Country codes are CZ, Czech Republic; DE, Germany; and PL, Poland. Major faults are LF, Lusatian Fault; ISF, Intra-Sudetic Fault; and SMF, Sudetic Marginal Fault. The displayed faults are a part of the Elbe Fault system, which has a complex history with alternating kinematics in response to stress variation since the late Carboniferous. The displayed fault kinematics are according to *Malkovský* [1987], *Oberc* [1991], and *Uličný* [2001]. (b) Shaded relief map of the Sudetes based on 90 m resolution SRTM digital elevation model (DEM) showing the morphologically distinct trace of the Sudetic Marginal Fault (SMF) and the location of the main study area (dashed rectangle), Krkonoše Mountains (KM), Góry Sowie Mountains (GSM), Rychlebské hory Mountains (RH) and city of Wroclaw, Poland, are shown for orientation.

[4] Previous low-temperature studies based primarily on bedrock apatite fission track data (~120–60°C sensitivity) [*Wagner and Van den Haute*, 1992] identified several cooling events throughout the Mesozoic-Cenozoic [*Jarmołowicz-Szulc*, 1984; *Wagner et al.*, 1989, 1997; *Hejl et al.*, 1997; *Coyle et al.*, 1997; *Thomson and Zeh*, 2000; *Glasmacher et al.*, 2002; *Ventura and Lisker*, 2003; *Aramowicz et al.*, 2006; *Filip et al.*, 2007; *Ventura et al.*, 2009; *Danišík et al.*, 2010]. These studies suggest that the Bohemian Massif experienced a complex thermal postorogenic evolution that may have been influenced by various processes. These include burial under sediments of Mesozoic intraplate basins, Late Cretaceous exhumation related to far field compression from the African-Iberian-European plates and/or reheating and exhumation related to the opening of the European Cenozoic Rift System in the Eocene-Oligocene. However, superposition of these processes often caused partial or total rejuvenation of thermochronological system(s) and consequently, ages obtained on bedrock samples using a single thermochronometer can be misleading. To circumvent the problem of the patchy geological record and the potential confusion introduced by multiple thermal events, an integrated approach, using multiple chronometers is warranted.

[5] The Rychlebské hory Mountain region in the NE Bohemian Massif provides a natural laboratory for studies of postorogenic evolution: first, this area, which forms an eastern part of the so-called Sudetes (Figure 1b), consists of a mosaic of fault-bounded basement blocks that were exhumed, uplifted and eroded to various levels, potentially recording different stages of thermal history. Second, the basement blocks are offset by the NW-SE striking Sudetic Marginal Fault (SMF), one of the morphologically most

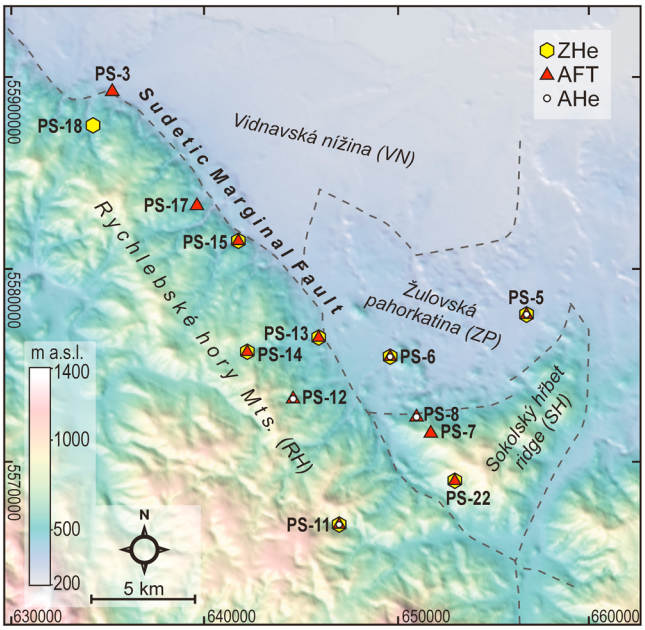

Figure 2. DEM of the main study area (in universal time meridian (UTM) zone 33 coordinate system) showing distribution of the major basement blocks, location of samples, and type of analyses conducted (ZHe, zircon (U-Th)/He dating; AFT, apatite fission track dating; AHe, apatite (U-Th)/He dating). Dashed lines show schematically the faults delineating the blocks.

prominent, but poorly understood features of central Europe's Elbe Fault system, which represents a regional-scale zone of crustal weakness with alternating kinematics since late Carboniferous [*Scheck et al.*, 2002]. The SMF controls a >140 km long escarpment separating the Sudetic Mountains from the foreland in the northeast (Figure 1). Third and perhaps most importantly, there are sparse remnants of postorogenic sediments of Cretaceous age preserved on some of the basement blocks within the Sudetes that can provide important constraints for landscape evolution studies.

[6] In this work, three low-temperature thermochronometers (zircon (U-Th)/He (ZHe), apatite fission track (AFT), and apatite (U-Th)/He (AHe)) are applied to the crystalline bedrocks as well as to the postorogenic Cretaceous sediments. By bracketing the ~200–40°C temperature range, these methods can constrain the timing, rate and style of postorogenic exhumation in the Rychlebské hory Mountains and enhance our understanding of paleoactivity along the SMF. A new evolutionary model for the Sudetes is presented that may also have implications for other seemingly controversial thermochronological data sets reported from other parts of the Bohemian Massif.

2. Morphological Setting and Geological Evolution

[7] The study area is located in the eastern part of the Sudetes. In general, it is composed of crystalline basement, dissected by faults into a mosaic of blocks uplifted to different elevations (Figure 1a). From the SE to the NW these blocks are (Figure 2): the Rychlebské hory Mountains (RH), the Sokolský hřbet (ridge) (SH), the Žulovská pahorkatina (hilly land) (ZP) and the Vidnavská nížina (lowland) (VN). The dominant structure is the NW-trending SMF which steeply dips to the NE (dip angle ~75°) [cf. *Štěpančíková et al.*, 2011a] and separates the RH in the footwall from the other three blocks (SH, ZP and VN) in the hanging wall (Figures 1 and 2).

[8] The RH block is a horstlike NW striking ridge, reaching a maximum altitude of 1127 m at sea level in its central parts. The wedge-shaped SH block is an asymmetric horst uplifted over 600 m toward the adjacent ZP block, which is a weathering surface of pre-Neogene age containing remnants of kaolin-rich saprolites [*Demek*, 1975, 1995; *Ivan*, 1983, 1997]. In the north, the down-thrown VN block, with a flat surface and slightly entrenched valleys, is delimited toward the ZP by up to ~40 m high fault scarps. It is a part of Neogene graben filled with terrestrial fluvial to lacustrine deposits up to 400 m thick [*Frejková*, 1968; *Ondra*, 1968; *Cwojdziński and Jodłowski*, 1978; *Dyjor*, 1983a; *Gabriel et al.*, 1982; *Cwojdziński and Żelaźniewicz*, 1995; *Badura et al.*, 2004].

[9] The basement blocks (RH, SH, and ZP) consist of medium-grade metamorphic volcano-sedimentary successions and granitoids formed during the Late Devonian-Carboniferous Variscan orogeny, when final collision of Gondwana with the northern continent of Laurussia occurred. This is documented by zircon and monazite U/Pb, Rb/Sr and Ar/Ar ages, clustering at 360–320 Ma [*Oberc-Dziedzic et al.*, 1996; *Szczepański*, 2002; *Zachovalová et al.*, 2002; *Turniak et al.*, 2006]. Based on stratigraphic relationships between Devonian metasediments, it is now accepted that the faults defining the block pattern within the Sudetes must have existed during the Variscan orogeny [*Cloos*, 1922; *Pouba and Mísař*, 1961] and that the Elbe Fault system acted as a dextral shearing zone [*Aleksandrowski et al.*, 1997; *Mattern*, 2001; *Scheck et al.*, 2002; *Mazur et al.*, 2006]. However, since the SMF did not produce any significant strike-slip displacement or ductile shearing at that time, it played only a minor role in the Variscan wrenching tectonics and could have originated as a Riedel-type brittle shear plane accompanying dextral movements on the major Intra-Sudetic Fault (Figure 1a) [*Aleksandrowski et al.*, 1997].

[10] Late stages of the Variscan orogeny (late Carboniferous–Early Permian) were characterized by rapid unroofing, uplift and erosion of the consolidated basement blocks. This is documented by bedrock Ar/Ar cooling ages on amphibole and mica (310–290 Ma) [*Maluski et al.*, 1995; *Schneider et al.*, 2006]. It can also be inferred from the thick (>1200–3000 m), coarsening-upward sequence of late Paleozoic sediments in the adjacent foreland and intramontane basins, which point to a Sudetic source and an increase in relief [*Berg*, 1938; *Malkovský*, 1987; *Mazur et al.*, 2006, 2010]. Fine-grained sandstones, siltstones, calcrete and gypsum horizons of Late Permian–Early Triassic age represent the last stage of intramontane molasse development and are interpreted as an indication of the peneplanation of the Sudetic basement blocks [*Lorenz and Mroczkowski*, 1978; *Malkovský*, 1987].

[11] With the exception of a few <100 m thick patches of Middle-Upper Jurassic limestone found in the S and NW of the Sudetes, no sediments of Middle Triassic to early Late Cretaceous age are known in the area [*Eliáš*,

1981; *Malkovský*, 1987]. The currently accepted view is that between ~230 and ~95 Ma, the Bohemian Massif, including the Sudetes, existed as an emerged, tectonically inactive landmass, subject to slow erosion and intense weathering, as evidenced by planation surfaces below the Late Cretaceous sediments and occurrences of thick kaolinic weathering mantles on the Paleozoic basement rocks [*Kroutilík and Skácel*, 1962; *Svoboda et al.*, 1964a; *Senkowiczowa*, 1970; *Malkovský*, 1979; *Migoń and Lidmar-Bergström*, 2001; *Badura et al.*, 2004].

[12] Tectonic activity resumed in the Late Cretaceous (Cenomanian) when a system of rapidly subsiding basins (so-called Bohemian Cretaceous Basin System) formed along reactivated Variscan shear zones of the Elbe Fault system during dextral transtension and at least ~1000 m of shallow marine sediments (fine gravels, cross-bedded sandstones, mudstones and marls) were deposited in the northern Bohemian Massif [*Skoček and Valečka*, 1983; *Wojewoda*, 1997; *Uličný*, 2001; *Scheck et al.*, 2002; *Uličný et al.*, 2003, 2009]. Paleogeographic reconstructions gave rise to the currently accepted view that the Sudetes formed two emerged areas (so-called 'Western and Eastern Sudetic Islands'), which supplied detritus to these basins at that time [*Scupin*, 1936; *Skoček and Valečka*, 1983; *Milewicz*, 1997; *Uličný*, 2001]. The extent of these 'Islands' is a matter of controversy as the amount of eroded Cretaceous strata has not been quantified and recent detrital mineralogical data do not support paleogeographic reconstructions [*Biernacka and Józefiak*, 2009].

[13] In the Late Cretaceous (85–70 Ma), the Bohemian Massif was affected by transpressional deformation induced by far-field stresses from the Europe-Iberia-Africa plate convergence [*Kley and Voigt*, 2008]. This led to the reactivation of NW-SE striking Variscan basement thrusts or transpressional faults within the Elbe Fault system with vertical offsets of several kilometers [*Scheck et al.*, 2002], the formation of thrust-related uplift and erosion of basement blocks and the inversion of the Cretaceous basins [*Kley and Voigt*, 2008]. This is evidenced by deformation of the Cretaceous strata, abrupt cessation of sedimentation in intramontane basins at ~80–85 Ma, and also by the distinct cooling phase recorded by thermochronological data in western and central parts of the Sudetes [*Svoboda et al.*, 1964b; *Skoček and Valečka*, 1983; *Jarmołowicz-Szulc*, 1984; *Ziegler*, 1987; *Wojewoda*, 1997; *Uličný*, 2001; *Aramowicz et al.*, 2006; *Ventura et al.*, 2009; *Danišík et al.*, 2010]. At present, the nearest occurrences of Cretaceous sediments (<~1000 m thickness) are found ~30 km W and E from the study area in the Intra-Sudetic Basin and Opole Basin, respectively (Figure 1b). Although there is no direct evidence of activity along the SMF, faulting documented at other Sudetic faults [*Malkovský*, 1987; *Schröder*, 1987; *Coubal*, 1990; *Zulauf and Duyster*, 1997; *Adamovič and Coubal*, 1999] may imply that the SMF was also active during the Late Cretaceous inversion.

[14] After the Late Cretaceous–early Paleogene inversion, peneplanation and weathering of the basement blocks occurred during the Paleogene-Miocene [*Svoboda et al.*, 1964b; *Oberc*, 1972; *Demek*, 1975; *Jahn*, 1980; *Král*, 1985; *Scheck et al.*, 2002; *Migoń and Lidmar-Bergström*, 2001]. This is evidenced by the general lack of Paleogene sediments in the Sudetes and by the presence of up to 100 m thick kaolinized bedrock profiles found below Miocene sequences in the boreholes north of the SMF [*Kužvart*, 1965; *Ondra*, 1968; *Walczak*, 1970; *Jahn*, 1980; *Kościówko*, 1982; *Jahn et al.*, 2000]. Beginning in the late Eocene, a SW-NE trending Eger rift associated with alkaline volcanism developed as an arm of the European Cenozoic Rift System in the NW part of the Bohemian Massif [*Dèzes et al.*, 2004]. Small basaltic intrusions are found on both side of the SMF and have been dated as Oligocene-Miocene and Pliocene in age (K/Ar ages: 30–18 Ma and ~5 Ma; [*Birkenmajer et al.*, 1977, 2002a, 2002b, 2004; *Badura et al.*, 2005; *Ulrych et al.*, 2011]).

[15] During the Miocene, differential subsidence resulting in widespread continental sedimentation in the Sudetes region commenced [*Oberc*, 1972; *Dyjor*, 1975, 1995]. The SMF was active as a normal fault with northeast-side-down throw during the Neogene as documented by displacement of Oligocene intrusions [*Birkenmajer et al.*, 1977; *Badura et al.*, 2007]. Close to the SMF, several tectonic grabens developed and were filled by sediments of fluviatile and limnic facies, reaching 300–600 m in thickness [*Oberc and Dyjor*, 1969; *Oberc*, 1972; *Dyjor*, 1983a; *Badura et al.*, 2004]. The intensive uplift of the footwall of the SMF is considered to have occurred as late as in the upper Miocene/Pliocene [*Oberc and Dyjor*, 1969; *Oberc*, 1972; *Dyjor*, 1975, 1983b, 1993] and Quaternary activity is evidenced by tectonic landforms, truncated Pleistocene fluvial terraces and offset Holocene colluvial deposits [*Krzyszkowski and Pijet*, 1993; *Mastalerz and Wojewoda*, 1993; *Dyjor*, 1995; *Krzyszkowski et al.*, 1995, 2000; *Krzyszkowski and Bowman*, 1997; *Ivan*, 1997; *Badura et al.*, 2003, 2007; *Štěpančíková et al.*, 2010, 2011b].

3. Samples and Methods

[16] Samples were collected at regular intervals over the three basement blocks (RH, SH and ZP), on the both sides of the fault (Figure 2). A total of 19 samples of Variscan granitic and metamorphic rocks were sampled; however, only 13 contained sufficient datable apatite and/or zircon. To investigate the possibility of Mesozoic burial in the area, two sandstone samples (PS-4 and PS-21) of Turonian age (~93 Ma) were collected from the nearest occurrences of Upper Cretaceous sediments located ~30 km east (Opole Basin) and west (Intra-Sudetic Basin, Figure 1b) of the study area. Sample PS-4 (Opole Basin) did not contain any apatite or zircon and could not be dated. One sample of kaolinized sand (PS-3) of Miocene age was collected from the downthrown side of the fault zone in order to constrain the amount of Neogene overburden (Figure 2).

[17] Apatite and zircon grains were separated using conventional magnetic and heavy liquid separation techniques. Fission track analysis was carried out using standard procedures described by *Danišík et al.* [2007]. The external detector method [*Gleadow*, 1981] was applied with the etching protocols of *Donelick et al.* [1999] for apatite (5.5 M HNO_3 for 20 s at 21°C) and the zeta calibration approach [*Hurford and Green*, 1983] was adopted to determine the ages. Fission track ages were calculated using TrackKey 4.2g [*Dunkl*, 2002]. Horizontal confined 'tracks in tracks' were measured in c axis parallel surfaces of apatite and were normalized for crystallographic angle using a c axis

projection [*Donelick et al.*, 1999; *Ketcham et al.*, 2007a]. The annealing properties of apatite were assessed by measuring D_{par} (the mean etch pit diameter of fission tracks measured on the apatite polished surface parallel to the crystallographic c axis) [*Burtner et al.*, 1994].

[18] For (U-Th)/He analysis, apatite and zircon crystals were hand picked following strict selection criteria [*Farley*, 2002; *Reiners*, 2005], then photographed and measured. Microscopic investigation and fission track analyses revealed that the vast majority of apatite crystals contained fluid inclusions and other impurities that might disturb the (U-Th)/He system and result in older than expected ages [*Ehlers and Farley*, 2003]. Extra effort was taken to select 'the least unsuitable' crystals for (U-Th)/He thermochronology. For each sample, up to 8 apatite and 3 zircon crystals of similar size and shape were selected for (U-Th)/He analysis. Apatite and zircon crystals were loaded in Pt and Nb tubes, respectively, degassed at ~960°C (apatite) and ~1250°C (zircon) under ultrahigh vacuum using laser heating, and analyzed for ^{4}He using the CSIRO Earth Science and Resource Engineering extraction line in the John de Laeter Centre of Isotope Research in Perth (Australia) on a Pfeiffer Prisma QMS-200 mass spectrometer. A "reextract" [*Farley*, 2002] was run after each sample to verify complete outgassing of the crystals and to test for the presence of undetected inclusions. If a sample exhibited residual gas in the reextract (i.e., >5% of original gas extraction), which was often the case for apatite crystals, it was considered to contain inclusions and was dismissed from further procedure. Following He measurements, the apatite and zircon grains were spiked with ^{233}U and ^{230}Th, dissolved following the procedure of *Evans et al.* [2005] and analyzed by isotope dilution inductively coupled mass spectrometry for ^{238}U and ^{232}Th on an Agilent 7500 ICP-MS.

[19] Total analytical uncertainty was calculated as the square root of the sum of the squares of weighted uncertainties on U, Th, and He measurements. Total analytical uncertainty was less than 4.5% in all cases and was used to calculate the error on raw (U-Th)/He ages. The raw AHe and ZHe ages were corrected for alpha ejection (F_t correction) after *Farley et al.* [1996] and *Hourigan et al.* [2005], respectively. A value of 5% was adopted as the uncertainty on the F_t correction and was used to calculate errors for the corrected AHe and ZHe ages. Single crystal He ages with associated analytical uncertainties were used to calculate the geometric mean as a representative number for each sample set using RadialPlotter [*Vermeesch*, 2009]. Replicate analyses of Durango apatite (23 analyses), measured over the period of this study as an internal standard and check of accuracy, yielded a mean (U-Th)/He age of 31.1 ± 0.9 Ma. This is in excellent agreement with the Durango (U-Th)/He age of 31.13 ± 1.01 Ma reported by *McDowell et al.* [2005].

[20] The low-temperature thermal history based on fission track and (U-Th)/He data was modeled using the HeFTy modeling program [*Ketcham*, 2005] operated with the multikinetic fission track annealing model of *Ketcham et al.* [2007b] (using D_{par} as a kinetic parameter) and the diffusion kinetics of zircon after *Reiners et al.* [2004].

4. Analytical and Modeling Results

[21] Results of the thermochronological analyses are summarized in Tables 1, 2, and 3 and shown in Figures 2, 3, 4, and 5. AFT ages are reported as central ages with 1σ errors while (U-Th)/He ages are reported as single grain ages with 1σ errors.

4.1. Zircon (U-Th)/He Data

[22] The ZHe ages determined for eight bedrock samples range from 364.9 ± 24.2 to 72 ± 4.5 Ma. Replicates of majority of samples reproduce well with all three single grain ages overlapping within analytical uncertainty. In two samples (PSZ-14 and PSZ-18), one replicate was distinctly different from the other two. Whereas the age of 364.9 ± 24.2 Ma in sample PSZ-14 can be straightforwardly excluded from the data set as it is older than U/Pb age of the granite (~320 Ma), the age of 117.9 ± 7.5 Ma for sample PSZ-18, clearly younger than other two replicates (184.7 ± 11.9 and 236.4 ± 15.1 Ma), is still considered geologically meaningful for the reasons described in the next paragraph.

[23] The ZHe ages form a distinct spatial pattern mimicking the distribution of the crustal blocks. Samples from the SH and ZP blocks NE of the SMF range from 117 to 96 Ma and from 91 to 72 Ma, respectively. These are clearly younger than Triassic-Jurassic ZHe ages from the RH block, SW of the SMF which range (with one exception as discussed below) from ~300 to ~190 Ma (Figure 3). This suggests that during the Late Cretaceous, the SH and ZP samples were residing at temperatures above ~180°C (ZHe closure isotherm) [*Reiners et al.*, 2004] while the RH samples were colder than ~180°C. The only exception within the RH block is sample PSZ-18, which yielded a Cretaceous ZHe age (117.9 ± 7.5 Ma) that overlaps with the ZHe age cluster for samples from the opposite side of the SMF. This sample revealed a positive correlation between the single grain ZHe ages and effective closure temperature of the crystals calculated using the Closure program of *Reiners and Brandon* [2006] (Figure 6). This indicates that the smallest grain, with the smallest diffusion domain (i.e., lowest closure temperature, ~178°C) may have been reset during the Late Cretaceous. This may also indicate that the other two zircon grains from the same sample with slightly higher closure temperatures, as well as the zircons from the other RH samples, were residing just above the ZHe closure isotherm in the Late Cretaceous.

4.2. Apatite Fission Track Data

[24] The bedrock samples (n = 11) yielded AFT ages between 80.6 ± 5 and 39 ± 4.4 Ma, all younger than corresponding ZHe ages and in accordance with the closure temperature concept [*Dodson*, 1973]. Nine samples, which passed the chi-square test and are thus considered to constitute one age population, form a loose cluster of Late Cretaceous to Eocene ages (80.6 ± 5.0–50.0 ± 3.7 Ma). Ages for samples PS-12 and PS-17 failed the chi-square test and show high dispersion (0.42 and 0.23, respectively). Age populations of 75.2 ± 9.2 and 27.1 ± 8.0 Ma (PS-12) and 64.4 ± 16.3 and 36.1 ± 10.0 Ma (PS-17) were identified using the PopShare software (Figures 4c and 4d) [*Dunkl and Székely*, 2003]. In contrast to ZHe ages, there is no difference in AFT ages among the basement blocks, suggesting their uniform cooling through the apatite partial annealing zone (~120–60°C) [*Gleadow et al.*, 1986a, 1986b; *Wagner and Van den Haute*, 1992].

[25] Both sediment samples yielded AFT ages indistinguishable from those of the bedrock samples, suggesting a

Table 1. Zircon (U-Th)/He Results[a]

	N_c	Th (ng)	Th (ng) Uncertainty (±%)	U (ng)	U (ng) Uncertainty (±%)	He (ncc)	He (ncc) Uncertainty (±%)	TAU (%)	Th/U	Uncorrected ZHe Age (Ma)	Uncorrected ZHe Age Uncertainty ±1σ (Ma)	F_t	Corrected ZHe Age (Ma)	Corrected ZHe Age Uncertainty ±1σ (Ma)[b]
PSZ-6 code														
PSZ-6-1	1	0.795	4.0	1.159	4.1	10.960	0.6	3.6	0.68	66.6	2.4	0.74	**90.1**	**5.5**
PSZ-6-2	1	0.617	4.1	1.046	4.1	9.587	0.6	3.7	0.59	65.8	2.4	0.72	**90.9**	**5.6**
PSZ-6-3	1	0.379	4.1	0.619	4.1	5.285	0.6	3.6	0.61	61.0	2.2	0.72	**85.3**	**5.3**
Central age													**88.7**	**3.0**
PSZ-5 code														
PSZ-5-1	1	0.575	4.4	1.170	4.5	8.323	0.6	4.1	0.49	52.2	2.1	0.67	77.6	5.0
PSZ-5-2	1	1.491	4.2	2.999	4.2	25.741	0.6	3.8	0.49	62.8	2.4	0.72	87.2	5.5
PSZ-5-3	1	0.317	4.3	0.573	4.2	3.729	0.6	3.8	0.55	47.2	1.8	0.65	72.0	4.5
Central age													78.7	7.7
PSZ-11 code														
PSZ-11-1	1	0.384	4.4	0.828	4.5	19.915	0.6	4.1	0.46	175.5	7.2	0.83	212.7	13.8
PSZ-11-2	1	0.290	4.3	0.710	4.2	16.130	0.6	3.9	0.41	167.8	6.5	0.80	210.8	13.3
PSZ-11-3	1	0.228	4.4	0.536	4.3	12.253	0.6	4.0	0.42	168.4	6.8	0.82	204.8	13.1
Central age													209.4	4.1
PSZ-13 code														
PSZ-13-1	1	0.141	4.3	1.171	4.2	23.231	0.6	4.1	0.12	156.3	6.4	0.82	190.4	12.3
PSZ-13-2	1	0.170	4.3	0.814	4.2	17.078	0.6	4.0	0.21	162.0	6.5	0.82	197.3	12.7
PSZ-13-3	1	0.236	4.3	1.066	4.2	22.306	0.6	4.1	0.22	161.1	6.6	0.81	199.6	12.9
Central age													195.7	4.8
PSZ-14 code														
PSZ-14-1[c]	1	0.250	4.5	1.855	4.4	65.587	0.6	4.4	0.13	274.4	11.9	0.75	364.9	24.2
PSZ-14-2	1	0.064	4.6	0.967	4.2	19.482	0.6	4.2	0.07	160.7	6.8	0.68	236.1	15.5
PSZ-14-3	1	0.126	4.4	0.927	4.4	22.041	0.6	4.3	0.13	186.2	8.0	0.70	264.3	17.4
Central age													249.8	20.0
PSZ-15 code														
PSZ-15-1	1	0.142	4.3	1.925	4.2	40.424	0.6	4.2	0.07	167.0	7.0	0.69	243.0	15.9
PSZ-15-2	1	0.344	4.0	2.082	4.0	54.600	0.6	3.9	0.16	203.6	8.0	0.76	269.5	17.2
PSZ-15-3	1	0.417	4.0	1.566	4.0	43.405	0.6	3.8	0.26	210.3	8.1	0.77	273.9	17.3
Central age													261.8	16.7
PSZ-18 code														
PSZ-18-1[c]	1	1.136	4.0	8.579	4.0	103.828	0.6	4.0	0.13	95.7	3.8	0.81	117.9	7.5
PSZ-18-2	1	0.703	4.0	5.910	4.0	151.672	0.6	4.0	0.12	201.4	8.0	0.85	236.4	15.1
PSZ-18-3	1	3.458	4.0	15.273	4.0	308.909	0.6	3.9	0.22	155.7	6.4	0.84	184.7	11.9
Central age													209.0	36.6
PSZ-22 code														
PSZ-22-1	1	0.500	4.3	1.664	4.2	21.365	0.6	4.0	0.30	97.7	3.9	0.83	117.3	8.6
PSZ-22-2	1	0.509	4.2	1.525	4.2	17.523	0.6	4.0	0.33	86.9	3.4	0.83	104.4	6.7
PSZ-22-3	1	0.340	4.3	1.406	4.2	12.558	0.6	4.0	0.24	69.1	2.8	0.72	95.6	6.1
Central age													105.4	10.9

[a] N_c, number of dated zircon crystals; Th, ^{232}Th; ng, nanogram; U, ^{238}U; He, ^{4}He in ncc at STP; ncc, nanocubic centimeter; TAU, total analytical uncertainty; F_t, alpha recoil correction factor after *Farley et al.* [1996] and *Hourigan et al.* [2005]. Central age was calculated using RadialPlotter program of *Vermeesch* [2009].

[b] Uncertainties of individual measurements are analytical errors. Uncertainties of central ages are calculated as standard deviations.

[c] Samples were excluded from the calculation of central age and standard deviation.

similar thermal history for all the samples. The AFT age of 57.4 ± 2.8 Ma revealed by the Turonian sandstone (PS-21) from the Intra-Sudetic Basin shows that the sample experienced temperatures high enough to reset the AFT chronometer postdeposition (Figure 4b). In contrast, the AFT age of the Miocene sand (PS-3) from the SMF zone is 58.0 ± 5.2 Ma (Figure 4a). This shows that the postdeposition Neogene temperatures were not high enough to reset the AFT system in the sample, which still records the thermal history of the source area.

[26] Track length distributions (Figure 5) of bedrock samples as well as of the Cretaceous sandstone sample (PS-21) are fairly similar with unimodal shapes, relatively short mean track lengths (MTL) of 12.1 to 13.3 μm and relatively large standard deviations (SD) of 1.3 to 1.7 μm. This suggests a similar thermal history with prolonged residence within the apatite partial annealing zone for all samples. The APAZ temperature estimate of 120–60°C is corroborated by the average D_{par} value ~1.6 μm measured in the majority of samples (Table 2), indicating a fluorine-rich apatite composition typified by relatively low annealing temperatures [*Wagner and Van den Haute*, 1992; *Carlson et al.*, 1999; *Ketcham et al.*, 1999].

Table 2. Apatite Fission Track Results and Geographic Coordinates of the Samples[a]

Code	Latitude[b]	Longitude[b]	Elevation (m above sea level)	Stratigraphic Age	Lithology	N	RhoS	Ns	RhoI	Ni	RhoD	Nd	$P(\chi^2)$ (%)	Disp.	Age (Ma)	$\pm1\sigma$ (Ma)	MTL (μm)	SD (μm)	NL	D_{par} (μm)
PS-3	N50°26'20.3"	E 6°54'24.2"	360	Miocene	kaolinized sand	20	5.743	218	11.222	426	7.184	3062	83	0.08	**58.0**	**5.2**				1.5
PS-4	N50°13'37.4"	E17°44'12.8"	282	Turonian	sandstone										**n/a**					
PS-5	N50°19'48.3"	E17°12'14.2"	321	Paleozoic	granite	25	3.178	375	5.279	623	6.971	3062	100	0.00	**65.5**	**4.5**				1.5
PS-6	N50°18'44.7"	E17°06'13.3"	370	Paleozoic	granite	25	2.185	294	4.586	617	6.714	3062	99	0.00	**50.0**	**3.7**	12.7	1.3	50	1.5
PS-7	N50°16'36.0"	E17°07'48.9"	704	Paleozoic	granite	25	4.882	509	6.502	678	6.885	3062	96	0.00	**80.6**	**5.0**				1.5
PS-8	N50°17'03.5"	E17°07'17.8"	498	Paleozoic	granite	30	14.679	1010	22.774	1567	6.800	3062	76	0.02	**68.4**	**3.1**				3.6
PS-11	N50°14'07.1"	E17°03'45.7"	693	Paleozoic	migmatite/orthogneiss	15	1.678	75	3.469	155	6.842	3062	100	0.00	**51.7**	**7.4**				1.5
PS-12	N50°17'41.1"	E17°01'51.6"	622	Paleozoic	migmatite/orthogneiss	23	8.118	337	24.882	1033	6.757	3062	0	0.42	**39.0**	**4.4**				4.3
PS-13	N50°19'18.7"	E17°03'04.9"	418	Paleozoic	migmatite/orthogneiss	30	24.185	1190	37.721	1856	6.928	3062	58	0.04	**69.4**	**3.0**	12.1	1.4	100	1.5
PS-14	N50°18'59.6"	E16°59'55.4"	598	Paleozoic	Migmatite/orthogneiss	27	6.764	533	10.190	803	6.672	3062	99	0.00	**69.1**	**4.1**	12.7	1.7	105	1.5
PS-15	N50°22'05.9"	E16°59'41.8"	385	Paleozoic	migmatite/orthogneiss	25	5.629	469	9.914	826	7.099	3062	93	0.00	**62.9**	**3.9**	12.5	1.3	93	1.5
PS-17	N50°23'06.1"	E16°57'54.8"	440	Paleozoic	orthogneiss	40	6.658	835	13.109	1644	7.056	3062	0	0.23	**56.2**	**3.4**				1.5
PS-18	N50°25'23.7"	E16°53'29.5"	449	Paleozoic	migmatite/orthogneiss										**n/a**					
PS-21	N50°24'32.5"	E16°25'31.1"	515	Turonian	sandstone	60	9.414	883	18.359	1722	7.141	3062	55	0.09	**57.4**	**2.8**				1.9
PS-22	N50°15'13.0"	E17°08'46.9"	745	Paleozoic	migmatite/orthogneiss	30	6.636	771	9.898	1150	7.013	3062	99	0.00	**73.3**	**3.8**	13.3	1.3	107	3.8

[a]N, number of dated apatite crystals; RhoS (RhoI), spontaneous (induced) track densities ($\times 10^5$ tracks/cm^2); Ns (Ni), number of counted spontaneous (induced) tracks; RhoD, dosimeter track density ($\times 10^5$ tracks/cm^2); Nd, number of tracks counted on dosimeter; $P(\chi^2)$, probability obtaining chi-square value (χ^2) for n degree of freedom (where n = number of crystals 1); Disp., dispersion; Age $\pm1\sigma$, central age ±1 standard error [*Galbraith and Laslett*, 1993]; MTL, mean track length; SD, standard deviation of track length distribution; NL, number of horizontal confined tracks measured; D_{par}, average etch pit diameter of fission tracks. Ages were calculated using zeta calibration method [*Hurford and Green*, 1983]; glass dosimeter CN-5, and zeta value of 313.7 $\pm$ 3.6 year/cm^2.
[b]WGS84.

4.3. Apatite (U-Th)/He Data

[27] Apatite from five bedrock samples were dated by (U-Th)/He methods. Single grain AHe ages ranging from 154.1 $\pm$ 8.9 to 50.8 $\pm$ 2.9 Ma are highly scattered and some are older than the corresponding ZHe ages (Table 3). Given the lack of correlation found between AHe ages and other parameters (such as crystal size or U and Th content) [*Shuster et al.*, 2006; *Flowers et al.*, 2009] and the no zoning of U observed in fission track mounts [*Meesters and Dunai*, 2002], the scatter and the 'too old' ages are assumed to have resulted from undetected imperfections in the analyzed crystals related to the initial quality problem of the apatite. After removing the 'too old' ages from the data set, the remaining AHe ages range from 105.5 $\pm$ 6.1 Ma to 50.8 $\pm$ 2.9 Ma and form a loose cluster at ~85 Ma.

[28] Several single grain AHe ages may appear to be older than the corresponding central AFT age which would conflict with the closure temperature concept [*Dodson*, 1973]. However, when compared to the single grain AFT ages following the recommendation of *Danišík et al.* [2010], all the AHe ages are within the range of the single grain AFT ages. Despite this justification and given the persistent scatter of AHe ages, interpretation of the AHe results remains difficult. The ZHe and AFT data are more consistent and robust than the AHe data so the latter are interpreted with great caution and are not included in thermal modeling.

4.4. Thermal History Modeling

[29] In order to reconstruct and interpret thermal trajectories that reconcile the thermochronological data, representative samples with >90 confined track lengths and reliable ZHe data were chosen for inverse thermal history modeling. The modeling results computed by HeFTy are critically dependent on predefined geological and thermal constraints [*Ketcham et al.*, 1999; *Ketcham*, 2005]. We converted the available information into time-temperature (tT) constraints and parameterized the model as follows (Figure 6).

[30] For the basement samples, the beginning of the tT path was set as T = 800–400°C at 320 Ma marking the time of basement consolidation in the late Paleozoic as recorded by higher-temperature geochronometers (U/Pb to Ar/Ar data). For sediment sample PS-21, the beginning of the path was set as T = 10°C at 95–90 Ma according to its age of deposition. The absence of a Middle Triassic–early Late Cretaceous geologic record in the Bohemian Massif, existence of basement weathering relicts of Mesozoic age and the onlap of Upper Cretaceous sediments onto the basement rocks all suggest that the basement blocks were residing at or close to the surface prior to the Late Cretaceous transgression. Accordingly, a tT constraint was set as T = 40–10°C at 120–90 Ma. During the early Late Cretaceous (Cenomanian), the Bohemian Cretaceous Basin System formed [*Skoček and Valečka*, 1983]. The reset Turonian sandstone sample and sedimentological data [*Biernacka and Józefiak*, 2009] imply that the area might have been buried under a significant pile of Cretaceous sediments. To test this hypothesis and to quantify the amount of overburden, a loose constraint of T = 20–300°C at 90–75 Ma was set into the model. A Cretaceous sedimentary record terminating abruptly at ~80 Ma, the lack of Paleogene sediments and the occurrence of kaolinized bedrock profiles found below the

Table 3. Apatite (U-Th)/He Results[a]

	N_c	Th (ng)	Th (ng) Uncertainty (±%)	U (ng)	U (ng) Uncertainty (±%)	He (ncc)	He (ncc) Uncertainty (±%)	TAU (%)	Th/U	Uncorrected AHe Age (Ma)	Uncorrected ZHe Age Uncertainty ±1σ (Ma)	F_t	Corrected AHe Age (Ma)	Corrected ZHe Age Uncertainty ±1σ (Ma)[b]	Single Grain AFT Age Range (Ma)
PS-5 code															
PS-5-1[c]	1	0.035	3.9	0.013	3.9	0.284	0.5	3.9	2.7085	108.5	3.1	0.70	**154.1**	**8.9**	44.6 ± 17.7–87.6 ± 23.6
PS-5-2[c]	1	0.030	3.8	0.038	3.9	0.471	0.5	3.9	0.7986	85.7	2.9	0.72	**119.5**	**7.2**	
PS-5-3[c]	1	0.026	3.8	0.012	3.9	0.149	0.5	3.9	2.2418	68.1	2.0	0.63	**108.9**	**6.3**	
PS-5-5	1	0.040	3.9	0.013	3.9	0.144	0.8	3.9	3.0631	53.0	1.5	0.61	**86.8**	**5.0**	
PS-5-6	1	0.026	3.8	0.174	3.8	0.704	0.6	3.9	0.1483	32.1	1.2	0.60	**53.6**	**3.4**	
PS-5-7	1	0.013	3.9	0.017	3.8	0.101	0.6	3.9	0.7584	39.9	1.3	0.58	**69.0**	**4.2**	
PS-5-8[c]	1	0.021	3.9	0.009	3.9	0.132	0.7	3.9	2.2861	78.2	2.3	0.78	**100.2**	**5.8**	
Central age													**68.6**	**16.6**	
PS-6 code															
PS-6-1[c]	1	0.073	3.8	0.031	3.9	0.552	0.5	3.9	2.3344	93.3	2.7	0.69	**134.3**	**7.8**	28.7 ± 18.7–78.5 ± 30.0
PS-6-2	1	0.133	3.8	0.054	3.9	0.486	0.7	3.9	2.4634	46.9	1.4	0.73	**64.1**	**3.7**	
PS-6-3	1	0.041	3.8	0.014	3.9	0.205	0.7	3.9	2.8900	70.4	2.0	0.67	**105.0**	**6.0**	
PS-6-4	1	0.031	3.9	0.013	3.9	0.121	0.7	3.9	2.4268	48.8	1.4	0.61	**80.1**	**4.6**	
PS-6-5[c]	1	0.041	3.8	0.024	3.8	0.426	0.6	3.9	1.6779	102.1	3.1	0.71	**143.8**	**8.4**	
PS-6-6	1	0.084	3.8	0.039	3.8	0.346	0.6	3.9	2.1670	48.5	1.4	0.65	**74.6**	**4.3**	
PS-6-7	1	0.028	3.8	0.010	3.9	0.111	0.5	3.9	2.8278	54.4	1.5	0.63	**86.3**	**5.0**	
Central age													**80.9**	**15.2**	
PS-8 code															
PS-8-1	1	0.010	4.0	0.127	3.9	1.227	0.6	3.9	0.0773	77.7	3.0	0.77	**101.1**	**6.4**	45.5 ± 11.9–92.6 ± 24.1
PS-8-2	1	0.012	3.9	0.168	3.9	1.416	0.6	3.9	0.0731	67.7	2.6	0.78	**87.0**	**5.5**	
PS-8-3[c]	1	0.069	3.8	0.093	3.9	1.275	0.6	3.9	0.7351	95.1	3.2	0.69	**137.1**	**8.3**	
PS-8-4	1	0.021	3.8	0.157	3.8	1.265	0.5	3.9	0.1357	63.7	2.4	0.75	**85.0**	**5.3**	
PS-8-5	1	0.122	3.8	0.069	3.8	0.933	0.5	3.9	1.7547	78.1	2.3	0.74	**105.5**	**6.1**	
PS-8-6	1	0.304	3.8	0.051	3.8	0.447	0.5	3.9	5.9640	30.0	0.8	0.59	**50.8**	**2.9**	
PS-8-7	1	0.017	4.1	0.058	3.8	0.449	0.5	3.9	0.2828	59.2	2.2	0.77	**76.9**	**4.8**	
Central age													**82.1**	**19.6**	
PS-11 and PS-12codes															
PS-11-3	1	0.008	4.3	0.010	3.9	0.089	0.7	4.0	0.8215	64.0	2.2	0.74	**86.6**	**5.2**	45.7 ± 23.8–85.3 ± 57.2
PS-12-1	1	0.006	4.2	0.896	3.9	7.098	0.5	3.9	0.0072	64.7	2.5	0.71	**91.6**	**5.8**	17.8 ± 4.2– 88.6 ± 30.1
PS-12-2	1	0.070	3.8	0.262	3.9	2.286	0.5	3.9	0.2635	67.1	2.5	0.80	**84.2**	**5.2**	
PS-12-3	1	0.040	3.8	0.165	3.9	1.409	0.5	3.9	0.2383	65.9	2.4	0.73	**90.4**	**5.6**	
PS-12-4	1	0.041	3.8	0.170	3.9	1.409	0.5	3.9	0.2390	64.3	2.4	0.67	**95.6**	**5.9**	
Central age													**90.4**	**4.7**	

[a] N_c, number of dated zircon crystals; Th, ^{232}Th; ng, nanogram; U, ^{238}U; He, ^{4}He in ncc at STP; ncc, nanocubic centimeter; TAU, total analytical uncertainty; F_t, alpha recoil correction factor after *Farley et al.* [1996]. Central age was calculated using RadialPlotter program of *Vermeesch* [2009].

[b] Uncertainties of individual measurements are analytical errors. Uncertainties of central ages are calculated as standard deviations.

[c] Samples were excluded from the calculation of central age and standard deviation.

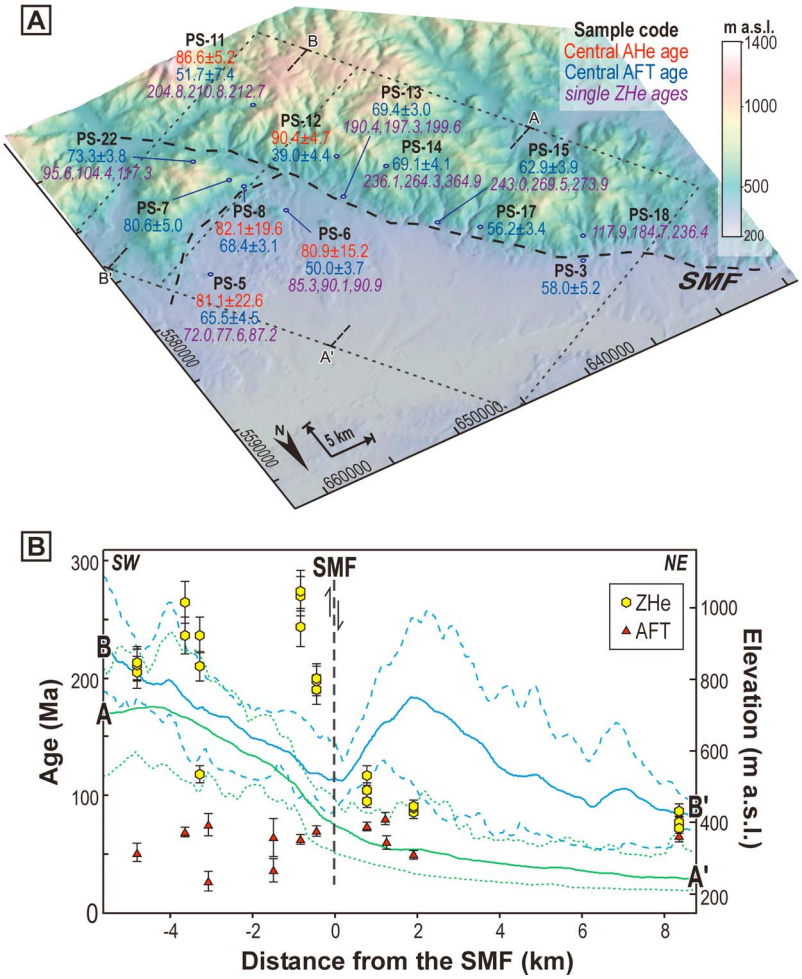

Figure 3. (a) Thermochronological results plotted on a DEM (UTM zone 33 coordinate system; orthogonal view from NE) and the location of two swath profiles (A-A′ and B-B′) displayed in Figure 3b. AHe age of sample PS-11 is based on one replicate. (b) Bedrock ZHe and AFT ages along the two swath profiles (A-A′, blue and B-B′, green; see Figure 3a for location) plotted as a function of distance from the SMF. Maximum, mean, and minimum elevation calculated from points sampled every 5 km along strike. For sample PS-12 and PS-17 the age populations identified by the PopShare software [*Dunkl and Székely*, 2003] are used as representative AFT ages. Note the remarkable offset of the ZHe data and no significant difference in the AFT data across the major fault.

Miocene sediments [*Ondra*, 1968; *Kościówko*, 1982] suggest that the basement blocks may have been exhumed to the surface during the Late Cretaceous–Paleogene. Accordingly, a tT constraint was set as T = 70–10°C at 80–40 Ma. To test the possibility of magmatic heating associated with Eger rift formation in the Oligocene-Miocene, a loose constraint of T = 10–100°C at 35–15 Ma was added to the model. The end of the tT path was set as T = 10°C at 0 Ma according to the present-day mean surface temperature [*Čermák et al.*, 2004].

[31] All the resultant modeled tT paths are characterized by a fairly similar cooling history comprising the following three stages (Figure 7): (1) rapid heating between 95 and 80 Ma at 10°C/Ma, peak temperatures of >110°C, 110–180°C, and >170°C for the Turonian sandstone sample (Figure 7d), the RH block (Figures 7a–7c), and the SH with ZP block (Figure 7e); (2) rapid cooling at ∼10°C/Ma to near-surface conditions between ∼85 and ∼60 Ma, and (3) slow cooling (∼1°C/Ma) or thermal stagnation lasting from 60 Ma until present, with the possibility of slight reheating (not exceeding ∼70°C) at ∼30–15 Ma (Figure 7).

5. Interpretation and Discussion

5.1. Exhumation and Erosion History

[32] Translation of the time-temperature paths into exhumation histories (Figure 8) requires a reasonable assumption of paleogeothermal gradient. Present-day geothermal gradients and heat flows in the area are on the order of 22–26°C/km and ∼50–55 mW m^{-2}, respectively, as estimated from borehole temperature and thermal conductivity measurements [*Bruszewska*, 2000; *Dowgiałło*, 2002; *Žák et al.*, 2006]. Since the local low relief of <600 m is unlikely to significantly perturb the thermal regime in the area [*Stüwe et al.*, 1994; *Mancktelow and Grasemann*, 1997; *Stüwe and Hintermüller*, 2000], we assume a uniform

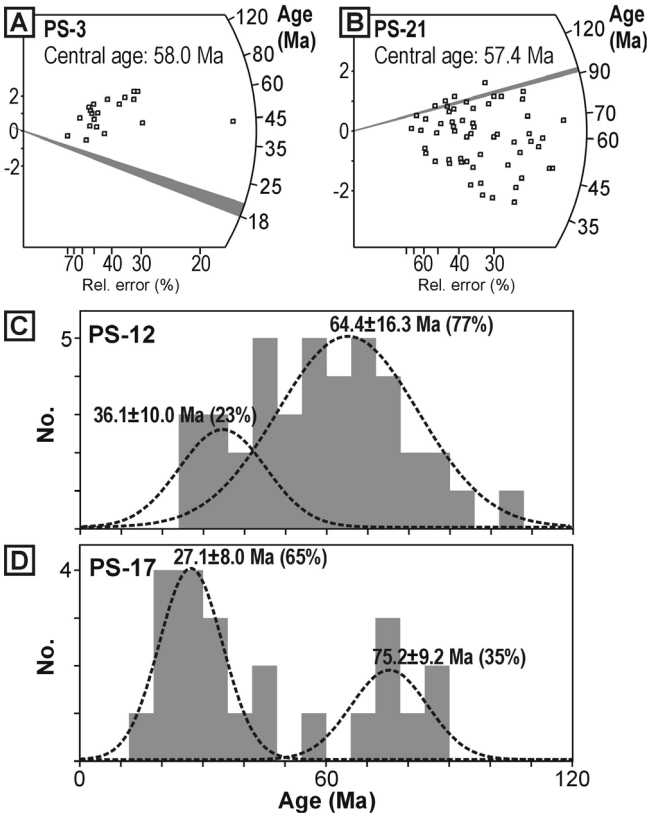

Figure 4. Radial plots of two sedimentary samples: (a) nonreset Miocene sandstone (PS-3) and (b) reset Cretaceous sandstone (PS-21). Depositional age is indicated by gray strips. Histograms of single grain ages of samples (c) PS-12 and (d) PS-17 with age populations (age, standard deviation, and fraction of grains belonging to the same age population) identified by the PopShare software [*Dunkl and Székely*, 2003].

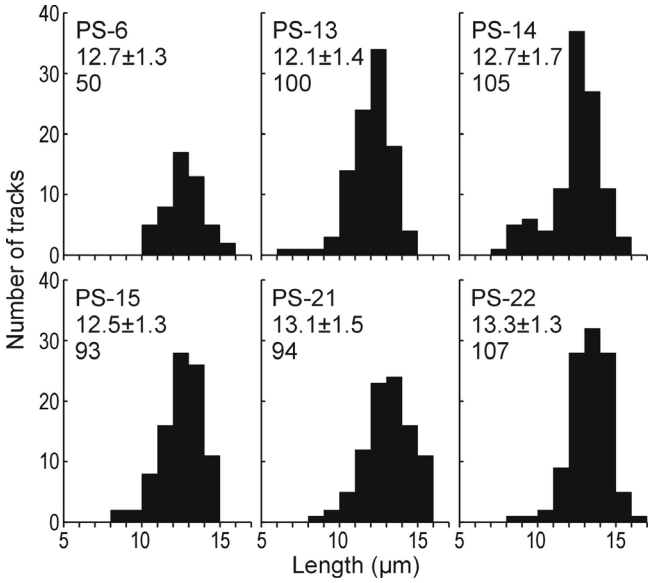

Figure 5. Apatite fission track length data. Shown in the top left in each histogram are sample code, mean track length ± standard deviation (both in μm), and number of measured tracks.

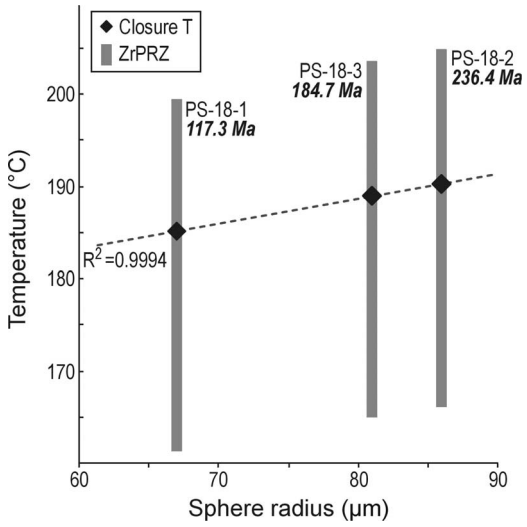

Figure 6. A positive correlation between diffusion domain size, ZHe age, and closure temperature and partial retention zone calculated for individual zircon crystals of sample PS-18. Note that the crystal with the youngest ZHe age (117.9 ± 7.5 Ma) is significantly smaller than the other two, which is in accord with the closure temperature concept. Diffusion domain size is expressed in terms of diameter of the sphere with the same surface to volume ratio as the dated crystals. Closure temperatures were calculated for cooling rate of 10°C/Ma using diffusion parameters for zircon after *Reiners et al.* [2004]. Ranges of zircon partial retention zone (ZHe PRZ) were calculated for time steps of 10 Myr, accounting for loss and production of He based on the accumulation-diffusion relation reported by *Wolf et al.* [1998].

paleogeothermal gradient of 24°C/km. It should be noted, however, that the geothermal gradient could have been increased during rift formation and associated volcanism in the Tertiary. The surface temperature is assumed to be 10°C according to the present-day mean surface temperature [*Čermák et al.*, 2004].

5.1.1. The Oldest ZHe Memory: Permo-Triassic Postorogenic Unroofing and Late Triassic–Early Cretaceous Thermal Inactivity

[33] The oldest low-temperature thermal history in the study area is recorded by the ZHe system in the RH block. ZHe ages range from ~300 to ~190 Ma but their interpretation is not straightforward due to the limited relevant geological record. The Permian-Triassic ZHe ages are slightly younger than the Ar/Ar ages of the basement and coincide with the age of sediments derived from the Sudetes and deposited in the Variscan molasse [*Malkovský*, 1987; *Mazur et al.*, 2006, 2010]. Therefore, we interpret the ZHe ages as cooling ages, recording postorogenic unroofing of the RH basement and its exhumation through the ZHe partial retention zone (ZHe PRZ: ~200–160°C) [*Reiners et al.*, 2004]. This interpretation implies that the major portion of the RH basement was ~7 km below the surface (assuming the ZHe closure

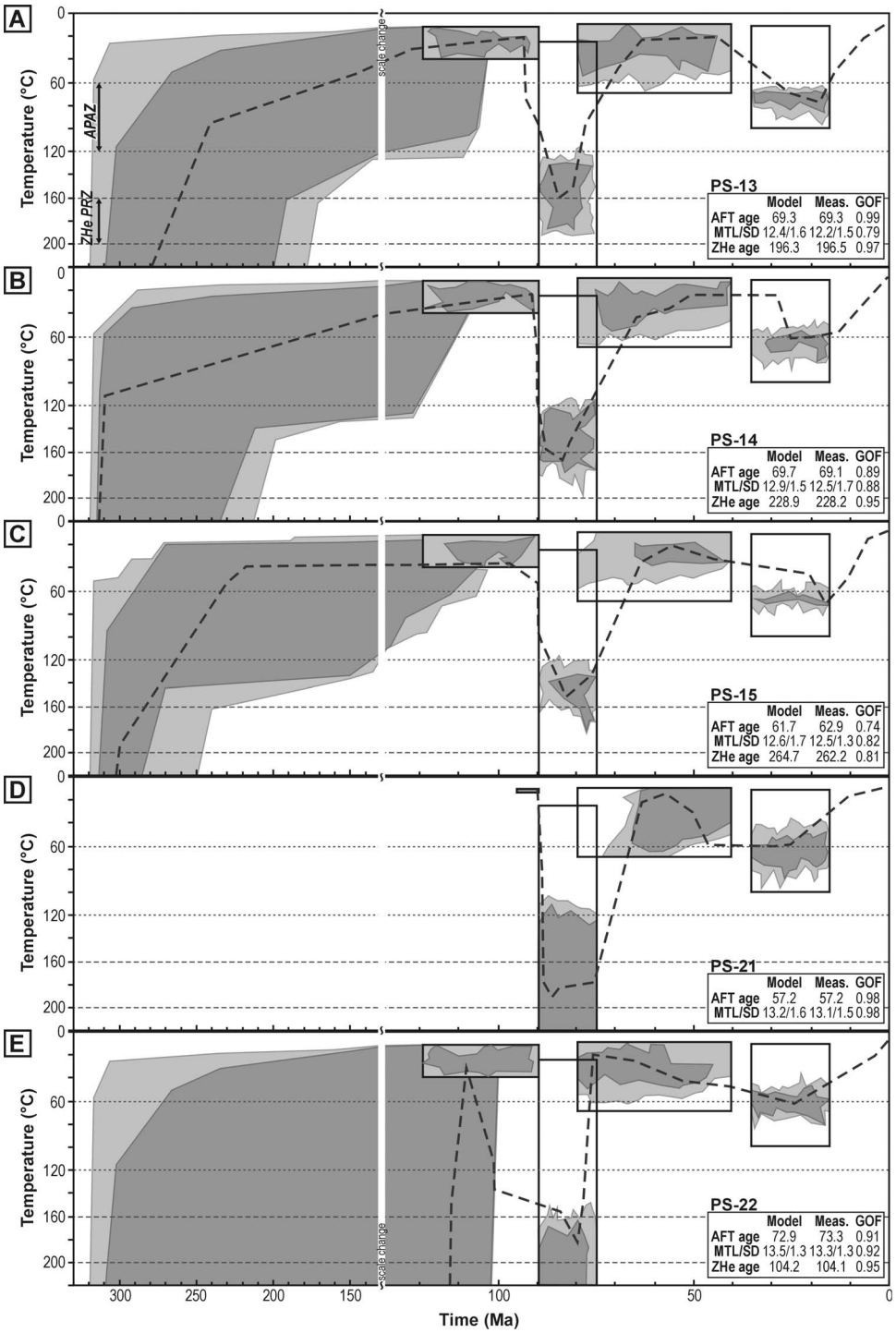

Figure 7. (a–e)Thermal modeling results of thermochronological data displayed in time-temperature diagrams modeled with the HeFTy program [*Ketcham*, 2005]. The best fit is shown as a dashed black line, shaded polygons (light grey, acceptable fit; dark grey, good fit) show the values of peak temperatures, and black rectangles represent constraints defined according to available geological record (see the text for details). ZHe PRZ, ZHe partial retention zone; APAZ, apatite partial annealing zone; MTL, mean track length in μm; SD, standard deviation in μm; GOF, goodness of fit (statistical comparison of the measured input data and modeled output data, where a "good" result corresponds to value 0.5 or higher, and "best" result corresponds to value 1). Note the difference in Cretaceous burial temperatures between samples SW (Figures 7a–7c) and NE (Figure 7e) of the SMF. Also note that pre-mid-Cretaceous thermal evolution is largely unconstrained at temperatures $<\sim$160°C as the AFT thermochronometer was fully reset in the mid-Cretaceous.

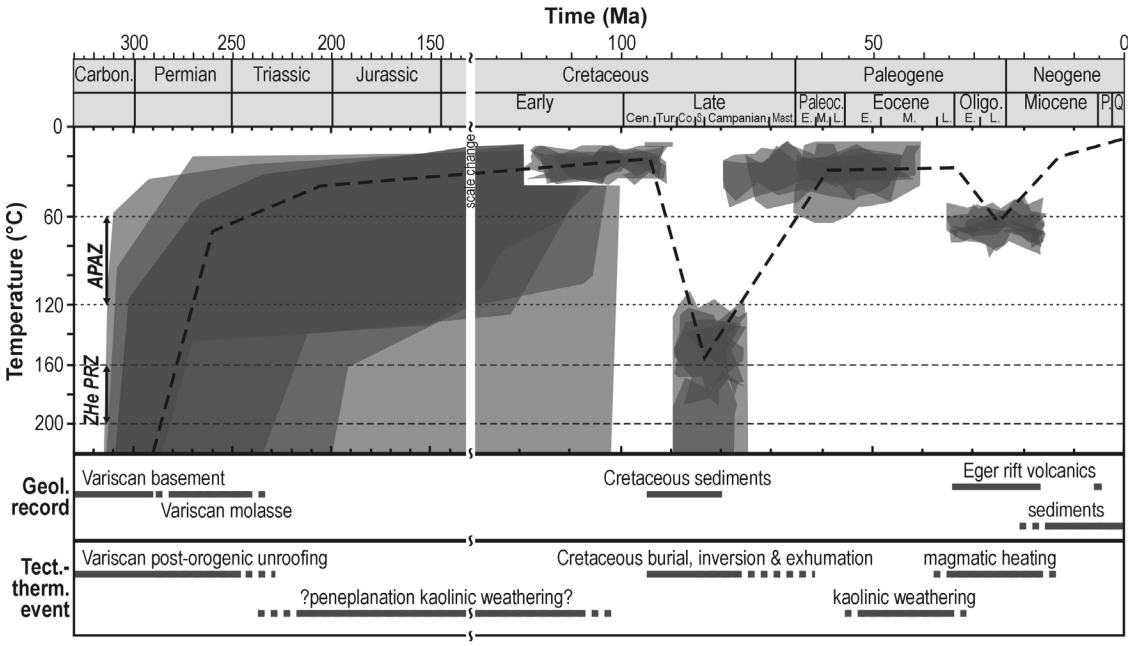

Figure 8. (top) Time-temperature diagram showing superimposed good fit thermal trajectories of all samples adopted from Figure 7. (middle) Available geological record in the Sudetes. (bottom) Major tectonothermal events in the Sudetes.

temperature ~180°C) in the Permian-Triassic and has never reached this depth since. The figure of ~7 km is our best estimate of the maximum post-Variscan erosion of the RH block.

[34] As there is no geological record of a thermal event of Late Triassic–Early Cretaceous age known from the Sudetes, we interpret the Jurassic ZHe ages as apparent ages, resulting from a partial reset of the ZHe system. In the absence of evidence or data to the contrary, we follow the model of other authors [e.g., *Svoboda et al.*, 1964a; *Senkowiczowa*, 1970; *Malkovský*, 1979; *Migoń and Lidmar-Bergström*, 2001; *Badura et al.*, 2004] and assume that in the Late Triassic–Early Cretaceous, the basement of the Sudetes, including the study area, formed an emerged landmass, undergoing slow erosion, surface lowering and weathering with the formation of thick weathering mantles (Figure 8).

5.1.2. Early Late Cretaceous Burial

[35] In the early Late Cretaceous (Cenomanian), the northern part of the Bohemian Massif was transgraded from the north by a shallow sea and sedimentary sequences (presently ~1100 m thick) were deposited in the subbasins of the Bohemian Cretaceous Basin system [e.g., *Skoček and Valečka*, 1983; *Wojewoda*, 1997; *Uličný*, 2001]. Significant parts of the Sudetes, including the study area, should have been exposed as islands within a shallow sea as stipulated by traditional paleogeographic models (Figure 9) [*Scupin*, 1913, 1936; *Milewicz*, 1997; *Skoček and Valečka*, 1983]. Our thermochronological data contradict this widely accepted opinion.

[36] First, the totally reset AFT system in the Turonian sandstone (PS-21) from the Intra-Sudetic Basin and the thermal modeling results clearly show temperatures >110°C at 90–75 Ma. This implies burial depths of >4 km during the Late Cretaceous transgression. Extrapolation of such thickness from the present-day sample location suggests a much greater lateral extent of the Intra-Sudetic Basin, which could have easily covered much a larger area of the Sudetes than assumed in the above mentioned models.

[37] Second, as evidenced by the fully reset AFT data, partially to fully reset ZHe data and by thermal modeling results of the bedrock samples, the studied basement bodies were definitely not on the surface during ~95–80 Ma period. Instead, they were rapidly heated to the temperatures of 110–180°C (RH block) and >170°C (SH and ZP blocks). In the case of the RH block, we tentatively argue that the maximum temperatures were closer to the zircon PRZ rather than apatite PAZ. This could be inferred from the Cretaceous ZHe age of 117.9 ± 7.5 Ma revealed by the smallest grain in sample PSZ-18, which has the lowest closure temperature (~178°C) (see section 4.1). We interpret the heating as recording basement burial by Cretaceous sediments to a depths of ~4–7 km (RH block) and >~6.5 km (SH and ZP blocks). We note that that maximum burial depth of the SH and ZP blocks could not have exceeded ~14 km as the white mica Ar/Ar system with the nominal closure temperature of 350°C [*McDougall and Harrison*, 1988] was not reset in the Cretaceous and preserves Variscan ages [*Szczepański*, 2002].

[38] There is, therefore, strong thermochronological evidence for a large and deep Late Cretaceous basin in the study area that covered a much larger portion of the Sudetes than assumed in the classic models of >5000 km^2 large, elongated "Eastern Sudetic Islands" [see *Scupin*, 1913, 1936; *Skoček and Valečka*, 1983; *Milewicz*, 1997]. In this basin, all 'subbasins' of the Bohemian Cretaceous Basin System (i.e., Intra-Sudetic Basin, Bohemian Cretaceous Basin, Opole Basin, North Sudetic Basin) were connected

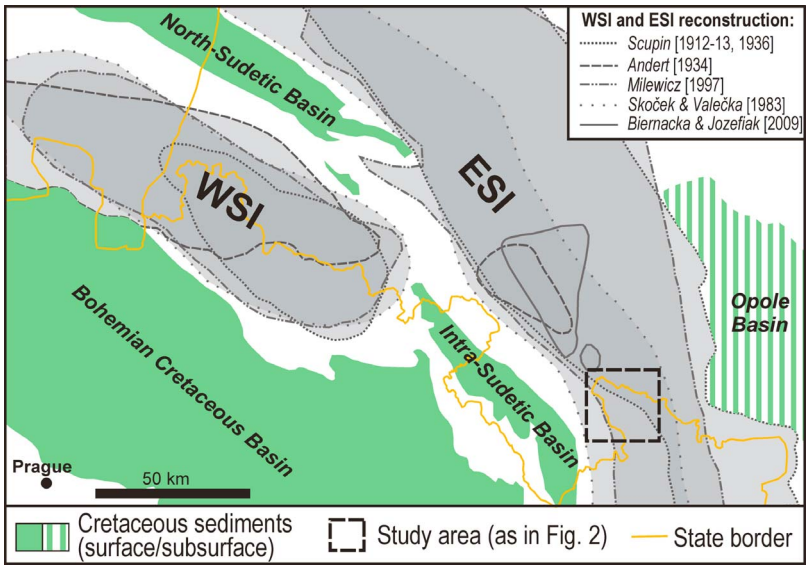

Figure 9. Paleogeographic position of the hypothetical eastern and western Sudetic Islands (ESI and WSI, respectively) during the early Turonian according to various authors (superimposed grey shaded areas), the present-day occurrences of the Cretaceous sediments (green), and the position of the study area (dashed rectangle). Our thermochronological data imply Cretaceous burial of the studied region, which contradicts the models of *Scupin* [1913, 1936], *Skoček and Valečka* [1983], and *Milewicz* [1997] but is in good agreement with the models of *Andert* [1934] and *Biernacka and Józefiak* [2009].

[*Klein et al.*, 1979; *Ziegler*, 1982; *Skoček and Valečka*, 1983; *Valečka and Skoček*, 1991] and should be seen in the present day as erosional relicts. This conclusion is in accord with the similar lithologies found in all the basins, pointing to their interconnection [*Klein et al.*, 1979; *Ziegler*, 1982; *Skoček and Valečka*, 1983; *Tarkowski*, 1991; *Valečka and Skoček*, 1991] and also with the heavy mineral assemblages in Cretaceous sediments, pointing to a much smaller, presumably <500 km^2 large source area, located in the Góry Sowie Massif (central Sudetes, Figure 1b) north of the SMF [*Biernacka and Józefiak*, 2009].

5.1.3. Early Late Cretaceous Inversion and Late Cretaceous–Paleocene Exhumation

[39] In the Late Cretaceous at 85–70 Ma, the Bohemian Massif was affected by the transpression related to Europe-Iberia-Africa plate convergence [*Kley and Voigt*, 2008]. This resulted in the inversion of the Cretaceous basin, local folding, upthrusting and exhumation of some basement blocks in the western parts of the Sudetes [*Adamovič and Coubal*, 1999; *Aramowicz et al.*, 2006; *Coubal*, 1990; *Uličný et al.*, 2003; *Mazur et al.*, 2005; *Ventura et al.*, 2009; *Ziegler and Dèzes*, 2007; *Danišík et al.*, 2010]. Both the distinct cluster of Late Cretaceous–Paleocene AFT ages found in the majority of our samples and the thermal modeling results show that the Late Cretaceous–Paleocene was indeed the main cooling period and the time when all the samples cooled from their maximum burial temperatures through the apatite PAZ (~120–60°C sensitivity) [*Wagner and Van den Haute*, 1992] to near-surface temperature conditions. We interpret this rapid cooling as recording the exhumation of the basement blocks related to the removal of the Cretaceous sedimentary cover.

[40] All basement blocks were exhumed at similar, relatively high exhumation rates of ~300 m/Ma, which may indicate that a tectonic component of the exhumation was facilitated by preexisting faults. As documented by ZHe data, the timing of the exhumation of the blocks through the zircon PRZ differed slightly: the RH block was exhumed from levels at the upper limit of the zircon PRZ and left the PRZ at ~118 Ma, the SH block passed the zircon PRZ at 117–95 Ma while the ZP block only passed the zircon PRZ at 90–72 Ma. This offset in ZHe ages and similar AFT ages found in all blocks suggest that the faults defining the basement blocks must have been active in the Late Cretaceous. This finding and its implication for the faulting history is discussed in more detail in section 5.3.

5.1.4. Eocene to Recent: Slow Cooling or Thermal Stagnation and Possible Slight Reheating

[41] Based on the lack of Paleogene sediments in the Sudetes and on the occurrence of kaolinized bedrock profiles preserved below the Miocene sequences north of the SMF, the whole Paleogene period is traditionally considered as another phase of peneplanation and weathering of the exposed basement blocks [*Oberc*, 1972; *Demek*, 1975; *Jahn*, 1980; *Kościówko*, 1982]. In general, our data support this interpretation, but also allow refinement of the timing of the weathering as follows: AFT ages of six samples fall into the Paleocene with one early Eocene age (Figure 3a and Table 2). These AFT ages, partly supported by the modeled thermal trajectories, show that at that the time these samples were cooling through the apatite PAZ so they were at depths of ~3–5 km and could not have been at the surface, being exposed to weathering as it has traditionally been assumed [*Kościówko*, 1982; *Walczak*, 1970; *Migoń*, 1997]. Instead we propose that the basement blocks reached the surface to begin weathering in the Eocene, at the earliest.

[42] From the Eocene to the present, the major portion of the basement blocks, with the exception of two samples

(PS-12, PS-17) discussed in the next paragraph, resided at temperatures <∼60°C. This is evidenced by the thermal modeling results and also by the AHe age of 154.1 ± 8.9–50.8 ± 2.9 Ma, which, despite the scatter, clearly document no resetting of the AHe thermochronometer after the early Eocene. The exact shape of the thermal trajectories during this period is, however, beyond the resolution of the results. The samples could have slowly cooled to surface conditions throughout the Tertiary, resided at the surface since the Eocene or experienced slight heating pulse(s) not exceeding ∼70°C. This interpretation implies that the amount of hypothetical Neogene burial in the study area could not have exceeded ∼1.5 km. This is supported by the 58.0 ± 5.2 Ma AFT age of the Miocene sandstone which clearly discounts the possibility of a significant Neogene burial.

[43] The only two complications to the interpretation above are samples PS-12 and PS-17, which yielded AFT populations of late Eocene and Oligocene age (36.1 ± 10.0 and 27.1 ± 8.0 Ma; see Figures 4c and 4d). Since these ages coincide with the opening of the Eger rift and emplacement of basaltoid intrusions in the surrounding of the study area [*Badura et al.*, 2007], they could be interpreted to record rift-related thermal activity. As we do not find any volcanic bodies in the vicinity of these samples, the likely cause of the thermal reset might have been some combination of hot fluid circulation, local thermal anomalies with increased heat flow, high thermal flux and/or heat emanated from some yet undiscovered subsurface magmatic bodies. Interestingly, there is no clear thermal signal of the late Eocene–Oligocene heating in the rest of the samples, although several samples did contain a few apatite grains of Oligocene AFT age (see also radial plot of PS-21, Figure 4b). These, however, are statistically insignificant when standard statistical treatment is applied. Therefore, we suggest that the late Eocene–Oligocene rift-related thermal event did not have a regional character and only caused local perturbations in the thermal regime.

[44] Finally, as there is no clear indication of a Neogene age in our data, we assume that late Cenozoic uplift and erosion of the basement blocks resulting in the present-day topography did not exceed a few hundred meters in the study area.

5.2. Implications for the Cretaceous Geodynamics of the Sudetes

[45] The Late Cretaceous has long been recognized as a period of major tectonic change in the Sudetes, which included rapid subsidence and inversion of sedimentary basins and uplift and erosion of crystalline basement bodies [*Skoček and Valečka*, 1983; *Coubal*, 1990; *Wojewoda*, 1997; *Uličný*, 2001; *Uličný et al.*, 2003; *Aramowicz et al.*, 2006; *Ziegler and Dèzes*, 2007; *Danišík et al.*, 2010]. A distinct cooling phase in the Late Cretaceous related to basement exhumation has been clearly documented by several studies.

[46] The pioneering study by *Jarmołowicz-Szulc* [1984], published early in the development of fission track methods, reported AFT ages ranging between 121 ± 10 and 63 ± 8 Ma from the Krkonoše Mountains. (western Sudetes, Figure 1b) and the adjacent areas to the north. These were interpreted as cooling ages, recording exhumation of the basement at ∼3 km depth in the mid-Cretaceous. *Aramowicz et al.* [2006] estimated Cretaceous/early Tertiary denudation of 4–8 km in Góry Sowie Mountains (central Sudetes, Figure 1b) based on thermal modeling of AFT data. Finally, *Danišík et al.* [2010] reported ZHe ages of 97 ± 7 to 86 ± 6 Ma from the Krkonoše Mountains (Figure 1b) and argued for post mid-Cretaceous exhumation of >6 km. It should be noted that all these studies utilized thermochronological data obtained on bedrock samples and that none could conclusively explain how and why the basement appeared at few kilometers depths prior to the Cretaceous exhumation or why the basement was not on the surface exposed to weathering as dictated by traditional paleogeographic reconstructions [*Scupin*, 1913, 1936; *Teisseyre*, 1960; *Skoček and Valečka*, 1983; *Milewicz*, 1997]. It should also be noted that some studies do hypothesize about the possibility of basement burial facilitated by a thick Variscan molasse [*Aramowicz et al.*, 2006], unspecified Mesozoic sediments [*Danišík et al.*, 2010] or by Cretaceous sediments [*Ventura et al.*, 2009], but in the absence of cogent arguments from posttectonic sediments, these hypotheses have remained speculative.

[47] Our multisystem thermochronology data on bedrock and sediment allow resolution of this issue by providing evidence for the existence of a huge basin in the Late Cretaceous. Sediments from this basin must have reached the thickness of several kilometers at some places and buried much larger parts of the northern Bohemian Massif than traditionally believed in the 'Sudetic Islands models'. Prior to the basin opening, it is entirely possible that the Sudetic basement bodies were close to the surface, exposed to weathering. But, as evidenced by the results of this and other studies mentioned above, at several places the basement must have been buried to significant depths with resultant temperatures high enough to reset the AFT, and in some cases even the ZHe thermochronometers.

[48] This finding has important implications for the interpretation and modeling strategies applied to thermochronological data from the Sudetes and other parts of the Bohemian Massif. The Mesozoic ages from the bedrocks should not be straightforwardly interpreted and modeled as cooling ages, reflecting simple cooling from hotter to colder temperature conditions. Instead, models should consider the possibility of ages representing reheating pulse(s).

5.3. Implications for SMF Activity

[49] As mentioned in section 2, the pre-Neogene faulting history of the SMF has not previously been clearly revealed. However, the distinct relationship between the thermochronological data on either side of the SMF allows three phases of fault activity and associated basement blocks displacement to be identified (Figure 10).

[50] ZHe ages SW and NE of the SMF are clearly offset; the footwall RH block (SW) retains pre-Cretaceous ages while the hanging wall (ZP and SH blocks) yields Late Cretaceous ages. Provided that the thermal regime on both sides of the fault is uniform [*Bruszewska*, 2000; *Dowgiałło*, 2002; *Žák et al.*, 2006], and the effect of the current topographic elevation differences on the ZHe system is negligible (sample elevations are comparable), the hanging wall with ZP and SH blocks must have resided at temperatures reflecting the ZHe PRZ in the Late Cretaceous. Since the reset was likely induced by deposition of sediments on the

basement blocks (see section 5.1.2), we argue that the ZP and SH blocks were displaced/thrown downward (subsided) along the SMF and that, therefore, the fault must have been active as a normal fault in the Late Cretaceous (Figure 10).

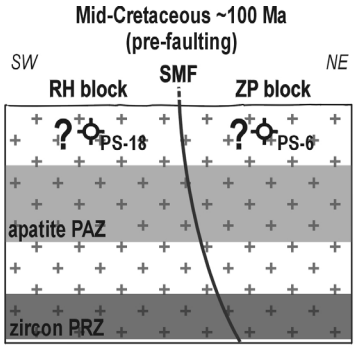

This corresponds with dextral transtension within the Elbe Fault system during that time and with the obliquity of the studied segment of the SMF relative to dextral strike slips such as Lusatian and Intra-Sudetic Fault [*Uličný*, 2001; *Scheck et al.*, 2002] (see Figure 1). The activity of the SMF was likely related to the far-field stresses emanating from Europe-Iberia-Africa plate convergence [*Kley and Voigt*, 2008].

[51] The uniform distribution of Paleogene AFT and AHe ages across the SMF suggests that all the blocks were cooling through the AFT and AHe partial retention zones at the same time. This implies that prior to entering the apatite PAZ, the downthrown hanging wall (ZP and SH blocks) were displaced to the same level as the footwall (RH block) (Figure 10). Thus, the SMF fault acted as a reverse fault during the early Late Cretaceous, which fits well to the inversion tectonics observed in other Sudetic faults and sedimentary basins [*Skoček and Valečka*, 1983; *Wojewoda*, 1997; *Adamovič and Coubal*, 1999; *Uličný*, 2001; *Scheck et al.*, 2002].

[52] Final uplift of the RH block along the SMF, leading to formation of the present-day horst and graben block topography, postdates cooling through the temperatures of AFT and AHe system closures. Therefore, the topography must be of late Cenozoic age. This finding is in good agreement with geological constraints, such as Oligocene intrusions cut by the SMF, triangular and trapezoidal facets along the RH block, truncated Pleistocene fluvial terraces and offset Holocene colluvium [*Grocholski*, 1977; *Dyjor*, 1975, 1983b, 1995; *Krzyszkowski and Pijet*, 1993; *Krzyszkowski et al.*, 1995, 2000; *Ivan*, 1997; *Krzyszkowski and Bowman*, 1997; *Mastalerz and Wojewoda*, 1993; *Badura et al.*, 2003, 2007; *Štěpančíková et al.*, 2010, 2011b].

6. Conclusions

[53] New ZHe, AFT and AHe data from the eastern part of the Sudetes provide important constraints on the tectonothermal evolution of the Sudetes and activity of the Sudetic Marginal Fault. The most significant results are summarized as follows:

[54] 1. Permian-Triassic ZHe ages found in the Rychlebské hory Mountains south of the SMF record RH basement cooling related to exhumation and postorogenic unroofing after the Variscan orogeny. The magnitude of post-Variscan erosion in the RH block is 7 km.

[55] 2. As evidenced by the resetting of the AFT thermochronometer in the Turonian sandstone, the study area was buried by a thick pile of sediments in the Late Cretaceous. Investigated basement blocks SW and NE of the SMF were buried to ~4–7 km and >6.5 km depths, respectively, as

Figure 10. Schematic illustration of the activity along the SMF as inferred from the thermochronological data, considering samples PS-18 and PS-6 as representatives for the RH and ZP blocks, respectively. The sense and relative magnitude of the vertical movements on the blocks is indicated by the arrows. Note that the position of the samples prior to Cretaceous burial is only assumed and not constrained by any data. Also note that the reverse faulting at ~80–60 Ma is only tentatively inferred from the similar AFT ages on the both side of the SMF.

evidenced by the full resetting of the AFT thermochronometer in all bedrock samples and the full resetting of the ZHe thermochronometer in bedrock samples NE of the SMF.

[56] 3. The extent of the Late Cretaceous basin suggested by our data contradicts the traditional "eastern Sudetic Island" which proposes large portions of emerged basement in a small Cretaceous sea [*Scupin*, 1913, 1936; *Skoček and Valečka*, 1983; *Milewicz*, 1997]. Instead, the data provided here support a much larger Cretaceous sea and regional burial of the Sudetes in the Cretaceous;

[57] 4. During late Late Cretaceous–Paleocene, the Late Cretaceous basin broke up with basement blocks rapidly exhumed from below the sedimentary cover to reach near-surface temperatures. This is evidenced by AFT ages of 80.6 ± 5.0 to 50.0 ± 3.7 Ma and thermal modeling results that suggest rapid cooling at that time.

[58] 5. Two samples record a slight reheating in the late Eocene and Oligocene, induced by thermal activity related to opening of the Eger rift and associated magmatism. This thermal event was of local importance as it was recorded in only two samples and did not manifest in either the AFT or the AHe system in the remaining samples.

[59] 6. The studied segment of the SMF acted as a normal fault during early Late Cretaceous burial, as a reverse fault during subsequent inversion and exhumation, and finally as a normal fault in the late Cenozoic. This is supported by nonoffset of the Late Cretaceous AFT ages and clear offset of the ZHe ages across the SMF resulting from different burial depths in the early Late Cretaceous.

[60] 7. Cretaceous ages in the Sudetes should be modeled as resulting from a reheating event.

[61] 8. Where possible, future thermochronological studies in the Sudetes, Bohemian Massif and other basement areas should focus on remnants of posttectonic sediments that may contain critically important clues needed to resolve often ambiguous thermal histories.

[62] **Acknowledgments.** We thank B. J. McDonald (CSIRO) for assistance with zircon dissolution and C. Scadding and A. Thomas (TSW Analytical) for assistance with ICP-MS. M.D. received financial support from the WA Geothermal Centre of Excellence. N.J.E. was supported by the Minerals Down Under Flagship. P.Š. was supported by the Czech Science Foundation, project 205/08/P521 and by the Institute Research Plan of the Institute of Rock Structure and Mechanics, Academy of Sciences of the Czech Republic, AVOZ30460519. The manuscript benefited from the constructive reviews by P. Monié and an anonymous reviewer.

References

Adamovič, J., and M. Coubal (1999), Intrusive geometries and Cenozoic stress history of the northern part of the Bohemian Massif, *Geolines*, *9*, 5–14.

Aleksandrowski, P., R. Kryza, S. Mazur, and J. Żaba (1997), Kinematic data on major Variscan strike-slip faults and shear zones in the Polish Sudetes, northeast Bohemian Massif, *Geol. Mag.*, *134*(5), 727–739, doi:10.1017/S0016756897007590.

Andert, H. (1934), Die Fazies in der Sudetischen Kreide unter besonderer Berücksichtigung des Elbsandsteingebirges, *Z. Dtsch. Ges. Geowiss.*, *86*, 617–637.

Aramowicz, A., A. A. Anczkiewicz, and S. Mazur (2006), Fission-track dating of apatite from the Góry Sowie Massif, Polish Sudetes, NE Bohemian Massif: Implications of post-Variscan denudation and uplift, *Neues Jahrb. Mineral Abh.*, *182*(3), 221–229, doi:10.1127/0077-7757/2006/0046.

Awdankiewicz, M., R. Kryza, and N. Rodionov (2010), SHRIMP zircon study of a micromonzodiorite dyke in the Karkonosze Granite, Sudetes (SW Poland): Age constraints for late Variscan magmatism in central Europe, *Geol. Mag.*, *147*(1), 77–85, doi:10.1017/S001675680999015X.

Badura, J., W. Zuchiewicz, A. Górecki, W. Sroka, B. Przybylski, and M. Żyszkowska (2003), Morphotectonic properties of the Sudetic Marginal Fault, SW Poland, *Acta Mont., Ser. A*, *24*(131), 21–49.

Badura, J., B. Przybylski, and W. Zuchiewicz (2004), Cainozoic evolution of Lower Silesia, SW Poland: A new interpretation in the light of sub-Cainozoic and sub-Quaternary topography, *Acta Geodyn. Geomater.*, *1*(3/135), 7–29.

Badura, J., Z. Pécskay, E. Koszowska, A. Wolska, W. Zuchiewicz, and B. Przybylski (2005), New age and petrological constraints on Lower Silesian basaltoids, SW Poland, *Acta Geodyn. Geomater.*, *2*(3/139), 7–15.

Badura, J., W. Zuchiewicz, P. Štěpančiková, B. Przybylski, B. Kontny, and S. Cacoń (2007), The Sudetic Marginal Fault: A young morphotectonic feature at the NE margin of the Bohemian Massif, central Europe, *Acta Geodyn. Geomater.*, *4*(4), 7–29.

Belton, D. X., R. W. Brown, B. P. Kohn, D. Fink, and K. A. Farley (2004), Quantitative resolution of the debate over antiquity of the central Australian landscape: Implications for the tectonic and geomorphic stability of cratonic interiors, *Earth Planet. Sci. Lett.*, *219*, 21–34, doi:10.1016/S0012-821X(03)00705-2.

Berg, G. (1938), *Erläuterungen zu Blatt Landeshut, Lieferung 193*, Preuss. Geol. Landesamt, Berlin.

Biernacka, J., and M. Józefiak (2009), The Eastern Sudetic Island in the early-to-middle Turonian: Evidence from heavy minerals in the Jerzmanice sandstones, SW Poland, *Acta Geol. Pol.*, *59*(4), 545–565.

Birkenmajer, K., M. Jeleńska, M. Kądziałko-Hofmokl, and J. Kruczyk (1977), Age of deep-seated fractures zones in Lower Silesia (Poland), based on K-Ar and paleomagnetic dating of Tertiary basalts, *Rocz. Pol. Tow. Geol.*, *47*(4), 545–552.

Birkenmajer, K., Z. Pécskay, J. Grabowski, M. W. Lorenc, and P. P. Zagożdżon (2002a), Radiometric dating of the Tertiary volcanics in Lower Silesia, Poland. II. K-Ar and palaeomagnetic data from Neogene basanites near Lądek Zdrój, Sudetes Mts., *Ann. Soc. Geol. Pol.*, *72*, 119–129.

Birkenmajer, K., Z. Pécskay, J. Grabowski, M. W. Lorenc, and P. P. Zagożdżon (2002b), Radiometric dating of the Tertiary volcanics in Lower Silesia, Poland. III. K-Ar and palaeomagnetic data from early Miocene basaltic rocks near Jawor, Fore-Sudetic Block, *Ann. Soc. Geol. Pol.*, *72*, 241–253.

Birkenmajer, K., Z. Pécskay, J. Grabowski, M. W. Lorenc, and P. P. Zagożdżon (2004), Radiometric dating of the Tertiary volcanics in Lower Silesia, Poland. IV. Further K-Ar and paleomagnetic data from late Oligocene to early Miocene basaltic rocks of the Fore-Sudetic block, *Ann. Soc. Geol. Pol.*, *74*, 1–19.

Bruszewska, B. (2000), The geothermal conditions in Lower Silesia (SW Poland), *Przegl. Geol.*, *48*(7), 639–643.

Burtner, R. L., A. Nigrini, and R. A. Donelick (1994), Thermochronology of Lower Cretaceous source rocks in the Idaho-Wyoming thrust belt, *AAPG Bull.*, *78*(10), 1613–1636.

Carlson, W. D., R. A. Donelick, and R. A. Kecham (1999), Variability of apatite fission-track annealing kinetics; I, Experimental results, *Am. Mineral.*, *84*, 1213–1223.

Cederbom, C., S. Å. Larson, E.-L. Tullborg, and J.-P. Stiberg (2000), Fission track thermochronology applied to Phanerozoic thermotectonic events in central and southern Sweden, *Tectonophysics*, *316*, 153–167, doi:10.1016/S0040-1951(99)00230-9.

Čermák, V., J. Šafanda, M. Krešl, and P. Dědeček (2004), Geotermika mapuje klimatické změny, *Cesk. Cas. Fyz.*, *54*(4), 244–246.

Cloos, H. (1922), *Der Gebirgsbau Schlesiens und die Stellung seiner Bodenschätze*, Gebrüder Borntraeger, Berlin.

Coubal, M. (1990), Compression along faults: Example from the Bohemian Cretaceous basin, *Miner. Slovaca*, *22*, 139–144.

Coyle, D. A., G. A. Wagner, E. Hejl, R. Brown, and P. Van den Haute (1997), The Cretaceous and younger thermal history of the KTB site (Germany): Apatite fission-track data from the Vorbohrung, *Geol. Rundsch.*, *86*, 203–209, doi:10.1007/s005310050132.

Cwojdziński, S., and S. Jodłowski (1978), Ukształtowanie powierzchni podłoża i geologia kenozoiku południowo-wschodniej części bloku przedsudeckiego, *Kwart. Geol.*, *22*(1), 181–193.

Cwojdziński, S., and A. Żelaźniewicz (1995), Podłoże krystaliczne bloku przedsudeckiego, paper presented at LXVI Annual Meeting, Geology and Environmental Protection of the Fore-Sudetic Block, Polish Geological Society, 11–28, Wrocław, Poland.

Cymerman, Z. (2004), Tectonic map of the Sudetes and Fore-Sudetic Block, 1:200,000, Panstw. Inst. Geol., Warsaw.

Czech Geological Survey (1998), Digital geoatlas of the Czech Republic, 1:500,000, Prague.

Danišík, M., J. Kuhlemann, I. Dunkl, B. Székely, and W. Frisch (2007), Burial and exhumation of Corsica (France) in the light of fission track data, *Tectonics*, *26*, TC1001, doi:10.1029/2005TC001938.

Danišík, M., R. F. Sachsenhofer, V. A. Privalov, E. A. Panova, W. Frisch, and C. Spiegel (2008), Low-temperature thermal evolution of the Azov Massif (Ukrainian Shield–Ukraine)—Implications for interpreting (U-Th)/He and fission track ages from cratons, *Tectonophysics*, *456*(3–4), 171–179, doi:10.1016/j.tecto.2008.04.022.

Danišík, M., P. Migoń, J. Kuhlemann, N. J. Evans, I. Dunkl, and W. Frisch (2010), Thermochronological constraints on the long-term erosional history of the Karkonosze Mts., central Europe, *Geomorphology*, *117*, 78–89, doi:10.1016/j.geomorph.2009.11.010.

Demek, J. (1975), Planation surfaces and their significance for the morphostructural analysis of the Czech Socialistic Republic (ČSR), *Stud. Geogr.*, *54*, 133–164.

Demek, J. (1995), Parallels between karst relief and granite relief: Case study of the Bohemian Highlands, Czech Republic, *Acta Mont., Ser. A*, *8*(97), 7–15.

Dèzes, P., S. M. Schmid, and P. A. Ziegler (2004), Evolution of the European Cenozoic Rift System: Interaction of the Alpine and Pyrenean orogens with their foreland lithosphere, *Tectonophysics*, *389*, 1–33, doi:10.1016/j.tecto.2004.06.011.

Dodson, M. H. (1973), Closure temperature in cooling geochronological and petrological systems, *Contrib. Mineral. Petrol.*, *40*, 259–274, doi:10.1007/BF00373790.

Donelick, R. A., R. A. Ketcham, and W. D. Carlson (1999), Variability of apatite fission-track annealing kinetics; II, Crystallographic orientation effects, *Am. Mineral.*, *84*(9), 1224–1234.

Dowgiałło, J. (2002), The Sudetic geothermal region of Poland, *Geothermics*, *31*, 343–359, doi:10.1016/S0375-6505(01)00037-2.

Dunkl, I. (2002), TRACKKEY: A Windows program for calculation and graphical presentation of fission track data, *Comput. Geosci.*, *28*(1), 3–12, doi:10.1016/S0098-3004(01)00024-3.

Dunkl, I., and B. Székely (2003), Component analysis with visualization of fitting—PopShare, a freeware program for evaluation of mixed geochronological data, *Geophys. Res. Abstr.*, *5*, 2657.

Dyjor, S. (1975), Młodoczwartorzędowe ruchy tektoniczne w Sudetach i na bloku przedsudeckim, in *Materiały I Krajowego Sympozjum "Współczesne i neotektoniczne ruchy skorupy ziemskiej w Polsce"*, pp. 121–132, Wydawn. Geol., Warsaw.

Dyjor, S. (1983a), Ewolucja trzeciorzędowych przedgórskich rowów tektonicznych centralnych i wschodnich Sudetów, in *Materiały Krajowego Sympozjum III, "Współczesne i neotektoniczne ruchy skorupy ziemskiej w Polsce,"* pp. 155–181, Wydawn. Geol., Wrocław, Poland.

Dyjor, S. (1983b), Problemy wieku dolnej granicy i faz ruchów neotektonicznych w południowo-zachodniej Polsce, in *Materiały Krajowego Sympozjum III, "Współczesne i neotektoniczne ruchy skorupy ziemskiej w Polsce,"* pp. 25–41, Wydawn. Geol., Wrocław, Poland.

Dyjor, S. (1993), Etapy blokowego rozwoju Sudetów i ich przedpola w neogenie i starszym czwartorzędedzie, *Folia Quarternaria*, *64*, 25–41.

Dyjor, S. (1995), Young Quaternary and recent crustal movements in Lower Silesia, SW Poland, *Folia Quarternaria*, *66*, 51–58.

Ehlers, T. A., and K. A. Farley (2003), Apatite (U-Th)/He thermochronometry: Methods and applications to problems in tectonic and surface processes, *Earth Planet. Sci. Lett.*, *206*(1–2), 1–14, doi:10.1016/S0012-821X(02)01069-5.

Eliáš, M. (1981), Facies and paleogeography of the Jurassic of the Bohemian Massif, *Sb. Geol. Ved. Geol.*, *35*, 75–155.

Evans, N. J., J. P. Byrne, J. T. Keegan, and L. E. Dotter (2005), Determination of uranium and thorium in zircon, apatite, and fluorite: Application to laser (U-Th)/He thermochronology, *J. Anal. Chem.*, *60*(12), 1159–1165, doi:10.1007/s10809-005-0260-1.

Farley, K. A. (2002), (U-Th)/He dating: Techniques, calibrations, and applications, *Rev. Mineral. Geochem.*, *47*, 819–844.

Farley, K. A., R. A. Wolf, and L. T. Silver (1996), The effect of long alpha-stopping distances on (U-Th)/He ages, *Geochim. Cosmochim. Acta*, *60*(21), 4223–4229, doi:10.1016/S0016-7037(96)00193-7.

Filip, J., and V. Suchý (2004), Thermal and tectonic history of the Barrandian lower Paleozoic, Czech Republic: Is there a fission-track evidence for Carboniferous-Permian overburden and pre-Westphalian alpinotype thrusting?, *Bull. Geosci.*, *79*(2), 107–112.

Filip, J., J. Ulrych, J. Adamovič, and K. Balogh (2007), Apatite fission track implications for timing of hydrothermal fluid flow in Tertiary volcanics of the Bohemian Massif, *J. Geosci.*, *52*, 211–220, doi:10.3190/jgeosci.014.

Flowers, R. M., R. A. Ketcham, D. L. Shuster, and K. A. Farley (2009), Apatite (U-Th)/He thermochronometry using a radiation damage accumulation and annealing model, *Geochim. Cosmochim. Acta*, *73*, 2347–2365, doi:10.1016/j.gca.2009.01.015.

Frejková, L. (1968), Žáruvzdorné jíly u Uhelné u Javorníka ve Slezsku, *Cas. Mineral. Geol.*, *13*, 167–173.

Gabriel, M., N. Gabrielová, Z. Hokr, E. Knobloch, and Z. Kvaček (1982), Miocén ve vrtu Vidnava Z-1, *Sb. Geol. Ved. Geol.*, *36*, 115–137.

Galbraith, R. F., and G. M. Laslett (1993), Statistical models for mixed fission track ages, *Nucl. Tracks Radiat. Meas.*, *21*, 459–470, doi:10.1016/1359-0189(93)90185-C.

Glasmacher, U., U. Mann, and G. A. Wagner (2002), Thermotectonic evolution of the Barrandian, Czech Republic, as revealed by apatite fission-track analysis, *Tectonophysics*, *359*, 381–402, doi:10.1016/S0040-1951(02)00538-3.

Gleadow, A. J. W. (1981), Fission-track dating methods: What are the real alternatives?, *Nucl. Tracks Radiat. Meas.*, *5*(1–2), 3–14.

Gleadow, A. J. W., I. R. Duddy, and P. F. Green (1986a), Fission track lengths in the apatite annealing zone and the interpretation of mixed ages, *Earth Planet. Sci. Lett.*, *78*, 245–254, doi:10.1016/0012-821X(86)90065-8.

Gleadow, A. J. W., I. R. Duddy, and P. F. Green (1986b), Confined fission track lengths in apatite: A diagnostic tool for thermal history analysis, *Contrib. Mineral. Petrol.*, *94*, 405–415, doi:10.1007/BF00376334.

Green, P. F., and I. R. Duddy (2006), Interpretation of apatite (U-Th)/He ages and fission track ages from cratons, *Earth Planet. Sci. Lett.*, *244*(3–4), 541–547, doi:10.1016/j.epsl.2006.02.024.

Grocholski, A. (1977), Uskok sudecki brzeżny a zagadnienie wulkanotektoniki trzeciorzędowej, *Pr. Geol. Mineral.*, *378*, 89–103.

Hejl, E., D. Coyle, N. Lal, P. Van den Haute, and G. A. Wagner (1997), Fission-track dating of the western border of the Bohemian Massif: Thermochronology and tectonic implications, *Geol. Rundsch.*, *86*, 210–219, doi:10.1007/s005310050133.

Hendriks, B. W. H., and T. F. Redfield (2005), Apatite fission track and (U-Th)/He data from Fennoscandia: An example of underestimation of fission track annealing in apatite, *Earth Planet. Sci. Lett.*, *236*, 443–458, doi:10.1016/j.epsl.2005.05.027.

Hourigan, J. K., P. W. Reiners, and M. T. Brandon (2005), U-Th zonation-dependent alpha-ejection in (U-Th)/He chronometry, *Geochim. Cosmochim. Acta*, *69*, 3349–3365, doi:10.1016/j.gca.2005.01.024.

Hurford, A. J., and P. F. Green (1983), The zeta age calibration of fission-track dating, *Chem. Geol.*, *41*, 285–317, doi:10.1016/S0009-2541(83)80026-6.

Ivan, A. (1983), Geomorfologické poměry Žulovské pahorkatiny, *Zpr. GgU CSAV*, *20*(4), 49–69.

Ivan, A. (1997), Topography of the Marginal Sudetic Fault in the Rychlebské hory Mts. and geomorphological aspects of epiplatform orogenesis in the NE part of the Bohemian Massif, *Moravian Geogr. Rep.*, *1*(5), 3–17.

Jahn, A. (1980), Tertiary relief of the Sudetes, *Geogr. Pol.*, *43*, 5–23.

Jahn, A., T. Chodak, P. Migoń, and C. August (2000), *Utwory Zwietrzelinowe Dolnego Ślaska. Nowe Stanowiska, Wiek i Znaczenie Geomorfologiczne*, *Stud. Geogr.*, vol. 72, pp. 210, Wydawn. Uniw. Wrocławskiego, Wrocław, Poland.

Janoušek, V., B. A. Wiegand, and J. Žák (2010), Dating the onset of Variscan crustal exhumation in the core of the Bohemian Massif: New U-Pb single zircon ages from the high-K calc-alkaline granodiorites of the Blatná suite, Central Bohemian Plutonic Complex, *J. Geol. Soc.*, *167*, 347–360, doi:10.1144/0016-76492009-008.

Jarmołowicz-Szulc, K. (1984), Geochronological study of a part of the northern cover of the Karkonosze granite by fission track method, *Arch. Mineral.*, *39*, 139–183.

Ketcham, R. A. (2005), Forward and inverse modeling of low-temperature thermochronometry data, in *Low-Temperature Thermochronology: Techniques, Interpretations, and Applications*, *Rev. Mineral. Geochem.*, vol. 58, edited by P. W. Reiners and T. A. Ehlers, pp. 275–314, Mineral. Soc. of Am., Chantilly, Va.

Ketcham, R. A., R. A. Donelick, and W. D. Carlson (1999), Variability of apatite fission track annealing kinetics: III. Extrapolation to geologic time scales, *Am. Mineral.*, *84*, 1235–1255.

Ketcham, R. A., A. Carter, R. A. Donelick, J. Barbarand, and A. J. Hurford (2007a), Improved measurement of fission-track annealing in apatite using c-axis projection, *Am. Mineral.*, *92*, 789–798, doi:10.2138/am.2007.2280.

Ketcham, R. A., A. Carter, R. A. Donelick, J. Barbarand, and A. J. Hurford (2007b), Improved modeling of fission-track annealing in apatite, *Am. Mineral.*, *92*, 799–810, doi:10.2138/am.2007.2281.

Klein, V., V. Müller, and J. Valečka (1979), Lithofazielle und palbgeographische Entwicklung des Bohmischen Kreidebeckens, in *Aspekte der Kreide Europas*, *Int. Union Geol. Sci. Ser. A*, vol. 6, pp. 435–446, Schweizerbart, Stuttgart, Germany.

Kley, J., and T. Voigt (2008), Late Cretaceous intraplate thrusting in central Europe: Effect of Africa-Iberia-Europe convergence, not Alpine collision, *Geology*, *36*(11), 839–842, doi:10.1130/G24930A.1.

Kościówko, H. (1982), Rozwój zwietrzelin kaolinowych na przedpolu Sudetów Wschodnich, *Biul. Inst. Geol.*, *336*, 7–52.

Košler, J., G. Rogers, J. C. Roddick, and D. R. Bowes (1995), Temporal association of ductile deformation and granitic plutonism: Rb-Sr and ^{40}Ar-^{39}Ar isotopic evidence from roof pendants above the Central Bohemian Pluton, Czech Republic, *J. Geol.*, *103*(6), 711–717.

Košler, J., S. Kelley, and S. Vrána (2001), ^{40}Ar/^{39}Ar hornblende dating of a microgranodiorite dyke: Implications for early Permian extension in the Moldanubian Zone of the Bohemian Massif, *Int. J. Earth Sci.*, *90*(2), 379–385, doi:10.1007/s005310000154.

Kotková, J., A. Kröner, W. Todt, and J. Fiala (1996), Zircon dating of North Bohemian granulites, Czech Republic: Further evidence for the Lower Carboniferous high-pressure event in the Bohemian Massif, *Geol. Rundsch.*, *85*, 154–161, doi:10.1007/s005310050064.

Král, V. (1985), *Zarovnané Povrchy České Vysočiny*, *Stud. CSAV*, vol. 10, Academia, Prague.

Kreuzer, H., E. Seidel, U. Schüssler, M. Okrusch, K.-L. Lenz, and H. Raschka (1989), K-Ar geochronology of different tectonic units at the northwestern margin of the Bohemian Massif, *Tectonophysics*, *157*(1–3), 149–178, doi:10.1016/0040-1951(89)90348-X.

Kröner, A., and E. Hegner (1998), Geochemistry, single zircon ages and Sm-Nd systematics of granitoid rocks from the Góry Sowie (Owl Mts), Polish West Sudetes: Evidence for early arc-related plutonism, *J. Geol. Soc.*, *155*(4), 711–724, doi:10.1144/gsjgs.155.4.0711.

Kröner, A., and A. Willner (1998), Time of formation and peak of Variscan HP-HT metamorphism of quartz-feldspar rocks in the central Erzgebirge, Saxony, Germany, *Contrib. Mineral. Petrol.*, *132*, 1–20, doi:10.1007/s004100050401.

Kroutilík, V., and J. Skácel (1962), Druhá zpráva o geologickém mapování na listu Slezské Rudoltice (list M-33-72-A Slezské Rudoltice a M-33-72-B–Matějovice), *Zpr. Geol. Vyzkumech Roce*, *1961*, 115–117.

Krzyszkowski, D., and D. Bowman (1997), Neotectonic deformation of Pleistocene deposits along the Sudetic Marginal Fault, southwestern Poland, *Earth Surf. Processes Landforms*, *22*, 545–562, doi:10.1002/(SICI)1096-9837(199706)22:6<545::AID-ESP712>3.0.CO;2-2.

Krzyszkowski, D., and E. Pijet (1993), Morphological effects of Pleistocene fault activity in the Sowie Mts., southwestern Poland, *Z. Geomorphol. Suppl.*, *94*, 243–259.

Krzyszkowski, D., P. Migoń, and W. Sroka (1995), Neotectonic Quaternary history of the Sudetic Marginal fault, SW Poland, *Folia Quaternaria*, *66*, 73–98.

Krzyszkowski, D., B. Przybylski, and J. Badura (2000), The role of neotectonics and glaciation on terrace formation along the Nysa Kłodzka River in the Sudeten Mountains (southwestern Poland), *Geomorphology*, *33*, 149–166, doi:10.1016/S0169-555X(99)00123-3.

Kužvart, M. (1965), Stáří zvětrávacích kůr, *Cas. Mineral. Geol.*, *10*(2), 197–200.

Lorenz, S., and J. Mroczkowski (1978), The sedimentation and petrography of Zechstein and lowermost Triassic deposits in the vicinity of Kochanow (Intra-Sudetic Trough), *Geol. Sudetica*, *13*(2), 23–39.

Malkovský, M. (1979), *Tektogeneze Platformního Pokryvu Českéo Masívu*, Ústred. Ústavu Geol., Praha.

Malkovský, M. (1987), Mesozoic and Tertiary basins of the Bohemian Massif and their evolution, *Tectonophysics*, *137*, 31–42, doi:10.1016/0040-1951(87)90311-8.

Maluski, H., P. Rajlich, and J. Souček (1995), Pre-Variscan, Variscan and early Alpine thermotectonic history of the north-eastern Bohemian Massif: ^{40}Ar/^{39}Ar study, *Geol. Rundsch.*, *84*, 345–358, doi:10.1007/BF00260445.

Mancktelow, N. S., and B. Grasemann (1997), Time-dependent effects of heat advection and topography on cooling histories during erosion, *Tectonophysics*, *270*, 167–195, doi:10.1016/S0040-1951(96)00279-X.

Mastalerz, K., and J. Wojewoda (1993), Alluvial-fan sedimentation along an active strike-slip fault: Plio-Pleistocene pre-Kaczawa fan, SW Poland, *Spec. Publ. Int. Assoc. Sedimentol.*, *17*, 293–304.

Mattern, F. (2001), Permo-Silesian movements between Baltica and western Europe: Tectonics and 'basin families,' *Terra Nova*, *13*(5), 368–375, doi:10.1046/j.1365-3121.2001.00368.x.

Mazur, S., P. Aleksandrowski, and J. Szczepański (2005), The presumed Teplá-Barrandian/Moldanubian terrane boundary in the Orlica Mountains (Sudetes, Bohemian Massif): Structural and petrological characteristics, *Lithos*, *82*, 85–112.

Mazur, S., P. Aleksandrowski, R. Kryza, and T. Oberc-Dziedzic (2006), The Variscan orogen in Poland, *Geol. Q.*, *50*, 89–118.

Mazur, S., A. Kröner, J. Szczepanski, K. Turniak, P. Hanžl, R. Melichar, N. V. Rodionov, I. Paderin, and S. A. Sergeev (2010), Single zircon U-Pb ages and geochemistry of granitoid gneisses from SW Poland: Evidence for an Avalonian affinity of the Brunian microcontinent, *Geol. Mag.*, *147*(4), 508–526, doi:10.1017/S001675680999080X.

McCann, T. (Ed.) (2008), *The Geology of Central Europe*, vol. 1, *Precambrian and Palaeozoic*, Geol. Soc., London.

McDougall, I., and T. M. Harrison (1988), *Geochronology and Thermochronology by the ^{40}Ar/^{39}Ar Method*, Oxford Univ. Press, New York.

McDowell, F. W., W. C. McIntosh, and K. A. Farley (2005), A precise ^{40}Ar-^{39}Ar reference age for the Durango apatite (U-Th)/He and fission-track dating standard, *Chem. Geol.*, *214*, 249–263, doi:10.1016/j.chemgeo.2004.10.002.

Meesters, A. G. C. A., and T. J. Dunai (2002), Solving the production-diffusion equation for finite diffusion domains of the various shapes: Part 1. Implications for low temperature (U-Th)/He thermochronology, *Chem. Geol.*, *186*(3–4), 333–344, doi:10.1016/S0009-2541(01)00422-3.

Migoń, P. (1997), Crystalline rock inselbergs in wouthwestern Poland, origin and paleoenvironmental significance, *Stud. Geogr.*, *66*, 1–92.

Migoń, P., and K. Lidmar-Bergström (2001), Weathering mantles and their significance for geomorphological evolution of central and northern Europe since the Mesozoic, *Earth Sci. Rev.*, *56*, 285–324, doi:10.1016/S0012-8252(01)00068-X.

Milewicz, J. (1997), Upper cretaceous of the North Sudetic Depression (litho- and biostratigraphy, paleogeography, tectonics and remarks on raw materials), *Pr. Geol. Mineral.*, *61*, 1–59.

Oberc, J. (1972), *Sudety i Obszary Przyległe, Budowa Geologiczna Polski*, vol. 4, *Tektonika, Part 2*, Wydawn. Geol., Warsaw.

Oberc, J. (1991), Systems of main longitudinal strike-slip faults in the vicinity of the Gory Sowie Block (Sudetes), *Kwart. Geol.*, *35*, 403–420.

Oberc, J., and S. Dyjor (1969), Uskok sudecki brzeżny, *Biul. Inst. Geol.*, *236*, 41–142.

Oberc-Dziedzic, T., C. Pin, J. K. Duthou, and J. P. Couterie (1996), Age and origin of the Strzelin granitoids (Fore-Sudetic Block, Poland): ^{87}Rb/^{86}Sr data, *Neues Jahrb. Mineral. Abh.*, *17*, 187–198.

Ondra, P. (1968), Zpráva o vrtném průzkumu miocenní pánve u Uhelné ve Slezsku, *Zpr. Geol. Vyzkumech Roce*, *1966*, 266–267.

Pouba, Z., and Z. Mísař (1961), O vlivu příčných zlomů na geologickou stavbu Hrubého Jeseníku, *Cas. Mineral. Petrol.*, *6*, 316–324.

Propach, G., A. Baumann, M. Schultz-Schmalschläger, and B. Grauert (2000), Zircon and monazite U-Pb ages of Variscan granitoid rocks and gneisses in the Moldanubian zone of eastern Bavaria, Germany, *Neues Jahrb. Geol. Palaeontol. Monatsh.*, *6*, 345–377.

Reiners, P. W. (2005), Zircon (U-Th)/He thermochronometry, in *Low-Temperature Thermochronology: Techniques, Interpretations, and Applications*, *Rev. Mineral. Geochem.*, vol. 58, edited by P. W. Reiners and T. A. Ehlers, pp. 151–176, Mineral. Soc. of Am., Chantilly, Va.

Reiners, P. W., and M. T. Brandon (2006), Using thermochronology to understand orogenic erosion, *Annu. Rev. Earth Planet. Sci.*, *34*, 419–466, doi:10.1146/annurev.earth.34.031405.125202.

Reiners, P. W., T. L. Spell, S. Nicolescu, and K. A. Zanetti (2004), Zircon (U-Th)/He thermochronometry: He diffusion and comparisons with ^{40}Ar/^{39}Ar dating, *Geochim. Cosmochim. Acta*, *68*, 1857–1887, doi:10.1016/j.gca.2003.10.021.

Scheck, M., U. Bayer, V. Otto, J. Lamarche, D. Banka, and T. Pharaoh (2002), The Elbe Fault System in north central Europe—A basement controlled zone of crustal weakness, *Tectonophysics*, *360*, 281–299, doi:10.1016/S0040-1951(02)00357-8.

Schneider, D. A., S. J. Zahniser, J. M. Glascock, S. M. Gordon, and M. Manecki (2006), Thermochronology of the west Sudetes (Bohemian Massif): Rapid and repeated eduction in the eastern Variscides, Poland and Czech Republic, *Am. J. Sci.*, *306*, 846–873, doi:10.2475/10.2006.03.

Schröder, B. (1987), Inversion tectonics along the western margin of the Bohemian Massif, *Tectonophysics*, *137*, 93–100, doi:10.1016/0040-1951(87)90316-7.

Schulmann, K., A. Kröner, E. Hegner, I. Wendt, J. Konopásek, O. Lexa, and P. Štípská (2005), Chronological constraints on the pre-orogenic history, burial and exhumation of deep-seated rocks along the eastern margin of the Variscan Orogen, Bohemian Massif, Czech Republic, *Am. J. Sci.*, *305*, 407–448, doi:10.2475/ajs.305.5.407.

Scupin, H. (1913), Die Löwenberger Kreide und ihre Fauna, *Palaeontographica*, *6*, suppl., 1–278.

Scupin, H. (1936), Zur palaeographie des Sudetischen Kreidemeeres, *Z. Dtsch. Ges. Geowiss.*, *88*, 309–325.

Senkowiczowa, H. (1970), Triassic (without Rhaetian deposits), in *Stratigraphy of the Mesozoic in the Margin of the Góry Świętokrzyskie*, *Biul. Inst. Geol.*, *56*, 21–35.

Shuster, D. L., R. M. Flowers, and K. A. Farley (2006), The influence of natural radiation damage on helium diffusion kinetics in apatite, *Earth Planet. Sci. Lett.*, *249*(3–4), 148–161, doi:10.1016/j.epsl.2006.07.028.

Siebel, W., C. K. Shang, E. Reitter, J. Rohrmüller, and K. Breiter (2008), Two distinctive granite suites in the southwestern Bohemian Massif and their record of emplacement: Constraints from geochemistry and $^{207}Pb/^{206}Pb$ chronology, *J. Petrol.*, *49*, 1853–1872, doi:10.1093/petrology/egn049.

Siebel, W., H. P. Hann, M. Danišík, C. K. Shang, C. Berthold, J. Rohrmüller, K. Wemmer, and N. J. Evans (2010), Age constraints on faulting and fault reactivation: A multi-chronological approach, *Int. J. Earth Sci.*, *99*, 1187–1197, doi:10.1007/s00531-009-0474-9.

Skoček, V., and J. Valečka (1983), Palaeogeography of the Late Cretaceous quadersandstein of central Europe, *Palaeogeogr. Palaeoclimatol. Palaeoecol.*, *44*, 71–92, doi:10.1016/0031-0182(83)90005-6.

Štěpančíková, P., J. Hók, D. Nývlt, J. Dohnal, I. Sýkorová, and J. Stemberk (2010), Active tectonics research using trenching technique on the southeastern section of the Sudetic Marginal Fault (NE Bohemian Massif, central Europe), *Tectonophysics*, *485*(1–4), 269–282, doi:10.1016/j.tecto.2010.01.004.

Štěpančíková, P., J. Dohnal, T. Pánek, M. Łój, V. Smolková, and K. Šilhán (2011a), The application of electrical resistivity tomography and gravimetric survey as useful tools in an active tectonics study of the Sudetic Marginal Fault (Bohemian Massif, central Europe), *J. Appl. Geophys.*, *74*(1), 69–80, doi:10.1016/j.jappgeo.2011.03.007.

Štěpančíková, P., D. Nývlt, J. Hók, and J. Dohnal (2011b), Paleoseismic study of the Sudetic Marginal Fault at the locality Bíla Voda (Bohemian Massif), paper presented at 2nd International Workshop on Active Tectonics, Earthquake Geology, Archaeology and Engineering, pp. 239–242, Int. Union for Quarternary Res., Corinth, Greece, 19–24 Sept.

Stüwe, K., and M. Hintermüller (2000), Topography and isotherms revisited: The influence of laterally migrating drainage divides, *Earth Planet. Sci. Lett.*, *184*, 287–303, doi:10.1016/S0012-821X(00)00315-0.

Stüwe, K., L. White, and R. Brown (1994), The influence of eroding topography on steady-state isotherms. Application to fission track analysis, *Earth Planet. Sci. Lett.*, *124*, 63–74, doi:10.1016/0012-821X(94)00068-9.

Svoboda, J., et al. (1964a), *Regionální Geologie ČSSR. Díl 1, Český Masív*, vol. 1, *Krystalinikum*, Ústřed. Ústavu Geol., Prague.

Svoboda, J., et al. (1964b), *Regionální Geologie ČSSR. Díl 1, Český Masív*, vol. 2, *Algonkium–Kvartér*, Ústřed. Ústavu Geol., Prague.

Szczepański, J. (2002), The $^{40}Ar/^{39}Ar$ cooling ages of white micas from the Jegłowa Beds (Strzelin Massif, Fore-Sudetic block, SW Poland), *Geol. Sudetica*, *34*, 1–7.

Tarkowski, R. (1991), *Stratygrafia, Makroskamieniałości i Paleogeografia Utworów Górnej Kredy Niecki Opolskiej*, *Zesz. Nauk. Akad. Goórn. Hutn. Stanisława Staszica*, vol. 1404, 1–156, Akad. Goórn. Hutn. im Stanisława Staszica, Krakow, Poland.

Teisseyre, H. (1960), Rozwój budowy geologicznej Sudetów od prekambru po trzeciorzed, in *Regionalna Geologia Polski*, vol. 3, *Sudety, Part 2, Utwory Trzeciorzędowe i Czwartorzędowe Oraz Pogląd na Rozwoój Budowy Geologicznej Sudetoó*, edited by H. Teisseyre, pp. 335–357, Pol. Tow. Geol., Krakow, Poland.

Thomson, S., and A. Zeh (2000), Fission-track thermochronology of the Ruhla Crystalline Complex: New constraints on the post-Variscan thermal evolution of the NW Saxo-Bohemian Massif, *Tectonophysics*, *324*(1–2), 17–35, doi:10.1016/S0040-1951(00)00113-X.

Turniak, K., M. Tichomirova, and K. Bombach (2006), Pb-evaporation zircon ages of post-tectonic granitoids from the Strzelin Massif (SW Poland), *Mineral. Pol. Spec. Pap.*, *29*, 212–215.

Uličný, D. (2001), Depositional systems and sequence stratigraphy of coarse-grained deltas in a shallow-marine, strike-slip setting: The Bohemian Cretaceous Basin, Czech Republic, *Sedimentology*, *48*, 599–628, doi:10.1046/j.1365-3091.2001.00381.x.

Uličný, D., S. Čech, and R. Grygar (2003), Tectonics and depositional systems of a shallow marine, intra-continental strike-slip basin: Exposures of the Český Ráj region, Bohemian Cretaceous Basin, *Geolines*, *16*, 133–148.

Uličný, D., L. Špičáková, R. Grygar, M. Svobodová, S. Čech, and J. Laurin (2009), Palaeodrainage systems at the basal unconformity of the Bohemian Cretaceous Basin: Roles of inherited fault systems and basement lithology during the onset of basin filling, *Bull. Geosci.*, *84*(4), 577–610, doi:10.3140/bull.geosci.1128.

Ulrych, J., J. Dostál, J. Adamovič, E. Jelínek, P. Špaček, E. Hegner, and K. Balogh (2011), Recurrent Cenozoic volcanic activity in the Bohemian Massif (Czech Republic), *Lithos*, *123*, 133–144, doi:10.1016/j.lithos.2010.12.008.

Valečka, J., and V. Skoček (1991), Late Cretaceous lithoevents in the Bohemian Cretaceous Basin, Czechoslovakia, *Cretaceous Res.*, *12*, 561–577, doi:10.1016/0195-6671(91)90031-7.

Ventura, B., and F. Lisker (2003), Long-term landscape evolution of the northeastern margin of the Bohemian Massif: Apatite fission-track data from the Erzgebirge (Germany), *Int. J. Earth Sci.*, *92*, 691–700, doi:10.1007/s00531-003-0344-9.

Ventura, B., F. Lisker, and J. Kopp (2009), Thermal and denudation history of the Lusatian Block (NE Bohemian Massif, Germany) as indicated by apatite fission-track data, *Geol. Soc. Spec. Publ.*, *324*, 181–192, doi:10.1144/SP324.14.

Vermeesch, P. (2009), RadialPlotter: A Java application for fission track, luminescence and other radial plots, *Radiat. Meas.*, *44*(4), 409–410, doi:10.1016/j.radmeas.2009.05.003.

Wagner, G. A., and P. Van den Haute (1992), *Fission-Track Dating*, Enke, Stuttgart, Germany.

Wagner, G. A., I. Michalsky, and P. Zaun (1989), Apatite fission-track dating of the central European basement, Postvariscan thermotectonic evolution, in *The German Continental Deep Drilling project (KTB)*, edited by R. Emmermann and J. Wohlenberg, pp. 481–500, Springer, New York.

Wagner, G. A., et al. (1997), Post-Variscan thermal and tectonic evolution of the KTB site and its surroundings, *J. Geophys. Res.*, *102*, 18,221–18,232, doi:10.1029/96JB02565.

Walczak, W. (1970), *Obszar Przedsudecki, Dolny Śląsk. Cz. II*, Państw. Wydawn. Nauk., Warsaw.

Wojewoda, J. (1997), Upper Cretaceous littoral-to-shelf succession in the Intrasudetic Basin and Nysa Trough, Sudety Mts., in *Obszary Źródłowe: Zapis w Osadach*, edited by J. Wojewoda, pp. 81–96, WIND, Wrocław, Poland.

Wolf, R. A., K. A. Farley, and D. M. Kass (1998), Modeling of the temperature sensitivity of the apatite (U-Th)/He thermochronometer, *Chem. Geol.*, *148*, 105–114, doi:10.1016/S0009-2541(98)00024-2.

Zachovalová, K., J. Leichmann, and J. Švancara (2002), Žulová Batholith: A post-orogenic, fractionated ilmenite-allanite I-type granite, *J. Czech Geol. Soc.*, *47*(1–2), 35–44.

Žák, J., B. Vyhnálek, and P. Kabele (2006), Is there a relationship between magmatic fabrics and brittle fractures in plutons? A view based on structural analysis, anisotropy of magnetic susceptibility and thermomechanical modelling of the Tanvald pluton (Bohemian Massif), *Phys. Earth Planet. Inter.*, *157*, 286–310.

Ziegler, P. A. (1982), *Geological Atlas of Western and Central Europe*, Elsevier, Amsterdam.

Ziegler, P. A. (1987), Late Cretaceous and Cenozoic intraplate compressional deformations in the Alpine foreland, *Tectonophysics*, *137*, 389–420, doi:10.1016/0040-1951(87)90330-1.

Ziegler, P. A., and P. Dèzes (2007), Cenozoic uplift of Variscan Massifs in the Alpine foreland: Timing and controlling mechanisms, *Global Planet. Change*, *58*(1–4), 237–269, doi:10.1016/j.gloplacha.2006.12.004.

Zulauf, G., and J. Duyster (1997), Supracrustal intraplate thickening of Variscan basement due to Alpine foreland compression: Results from the superdeep well KTB (Bohemian Massif, Germany), *Tectonics*, *16*(5), 730–743, doi:10.1029/97TC01656.

M. Danišík, Department of Earth and Ocean Sciences, University of Waikato, Private Bag 3105, Hamilton 3240, New Zealand. (m.danisik@waikato.ac.nz)

N. J. Evans, CSIRO Earth Science and Resource Engineering, ARRC, 26 Dick Perry Ave., Kensingston, WA 6151, Australia. (noreen.evans@csiro.au)

P. Štěpančíková, Department of Engineering Geology, Institute of Rock Structure and Mechanics, Academy of Sciences of the Czech Republic, V Holešovičkách 41, 18209 Prague 8, Czech Republic. (stepancikova@irsm.cas.cz)